Dynamics of Newtonian Annular Jets

D.D. Paul

January 1979

UWFDM-287

FUSION TECHNOLOGY INSTITUTE

UNIVERSITY OF WISCONSIN

MADISON WISCONSIN

Dynamics of Newtonian Annular Jets

D.D. Paul

Fusion Technology Institute
University of Wisconsin
1500 Engineering Drive
Madison, WI 53706

http://fti.neep.wisc.edu

January 1979

UWFDM-287

DYNAMICS OF NEWTONIAN ANNULAR JETS

D.D. PAUL

DECEMBER 1978

Fusion Research Program
Nuclear Engineering Department
University of Wisconsin
Madison WI 53706 U.S.A.

UWFDM-287

ACKNOWLEDGEMENTS

This report is based on a MS thesis prepared for the Nuclear Engineering Department at the University of Wisconsin under the supervision of Professor S.I. Abdel-Khalik.

I would like to express my sincere appreciation to Professor S.I. Abdel-Khalik for his guidance and encouragement throughout all phases of this work.

My special thanks to the Department of Nuclear Engineering for providing the materials used to construct the experimental appartus, and to the Department of Energy for providing a traineeship for my studies.

This work has been partially funded by the Department of Energy.

TABLE OF CONTENTS

LIST OF TABLES

LIST OF FIGURES

SUMMARY

The main objectives of this investigation are to identify the significant parameters affecting the dynamics of Newtonian annular jets, and to develop theoretical models for jet break-up and collapse. This study has been motivated by recent developments in laser-fusion reactor designs; one proposed cavity design involves the use of an annular lithium jet to protect the cavity wall from the pellet debris emanating from the microexplosion.

An annular jet of fluid has two free surfaces: one on the inside and one on the outside of the annulus. Two methods of producing annular jets are discussed. In the first method, a sharp-edged orifice is used to produce an annular jet with a nearly uniform velocity distribution at the nozzle exit. In the second method, the fluid is forced to flow between two concentric cylinders which are long enough to insure that the velocity distribution is fully developed at the nozzle exit. It was found experimentally that the nozzle design, i.e. the initial velocity distribution in the jet, is an important parameter affecting the jet collapse and break-up.

An experimental apparatus was constructed to examine the behavior of annular water jets flowing in air with or without axial air flow through the center of the jet. A sharp-edged orifice nozzle was used to produce the annular jet. The nozzle was designed such that air could be injected into the center of the nozzle at a known flow rate. Two distinct types of jet behavior were observed. When the center of the annulus was vented to the atmosphere, the annular jet collapsed into a solid circular jet within 1 to 2 nozzle diameters.

However, when air was injected into the center of the annulus at a rate such that the air velocity was approximately equal to the average water velocity, the annular jet was observed to break-up uniformily into hollow spherical shells.

Theories are presented which satisfactorily explain the modes of jet break-up and the phenomenon of jet collapse.

CHAPTER 1

INTRODUCTION

Recent developments in the laser-fusion reactors design area have generated considerable interest in the study of annular jet dynamics. The "liquid lithium waterfall" concept proposed by the Lawrence Livermore Laboratory [1,2] involves the use of an annular lithium jet to protect the cavity wall from the pellet debris and x-rays emanating from the microexplosion. A schematic diagram of the lithium waterfall cavity design is shown in Fig. 1-1. The principal feature of this concept is a thick continuously recyclable first wall of lithium. On each pellet explosion, the annular jet is disassembled and is then re-established. The lithium is continuously pumped to the top of the vacuum chamber through a reservoir region which separates the first wall from the pressure vessel. A small fraction of the lithium in the fall and reservoir regions is circulated to the heat exchangers which in turn transfers heat to the steam generation cycle. Liquid lithium serves as the primary coolant, neutron moderator, and the fertile material for tritium breeding.

The lithium waterfall concept appears to offer several advantages over other cavity designs proposed to date; however, many questions remain to be answered before its feasibility can be established [3]. The dynamics of the lithium fall is the main uncertainty involved in this concept. It must be shown that at the required velocity and thickness, the jet will not collapse or disassemble prior to reaching the bottom of the cavity. This investigation

LIQUID LITHIUM "WATERFALL" CONCEPT

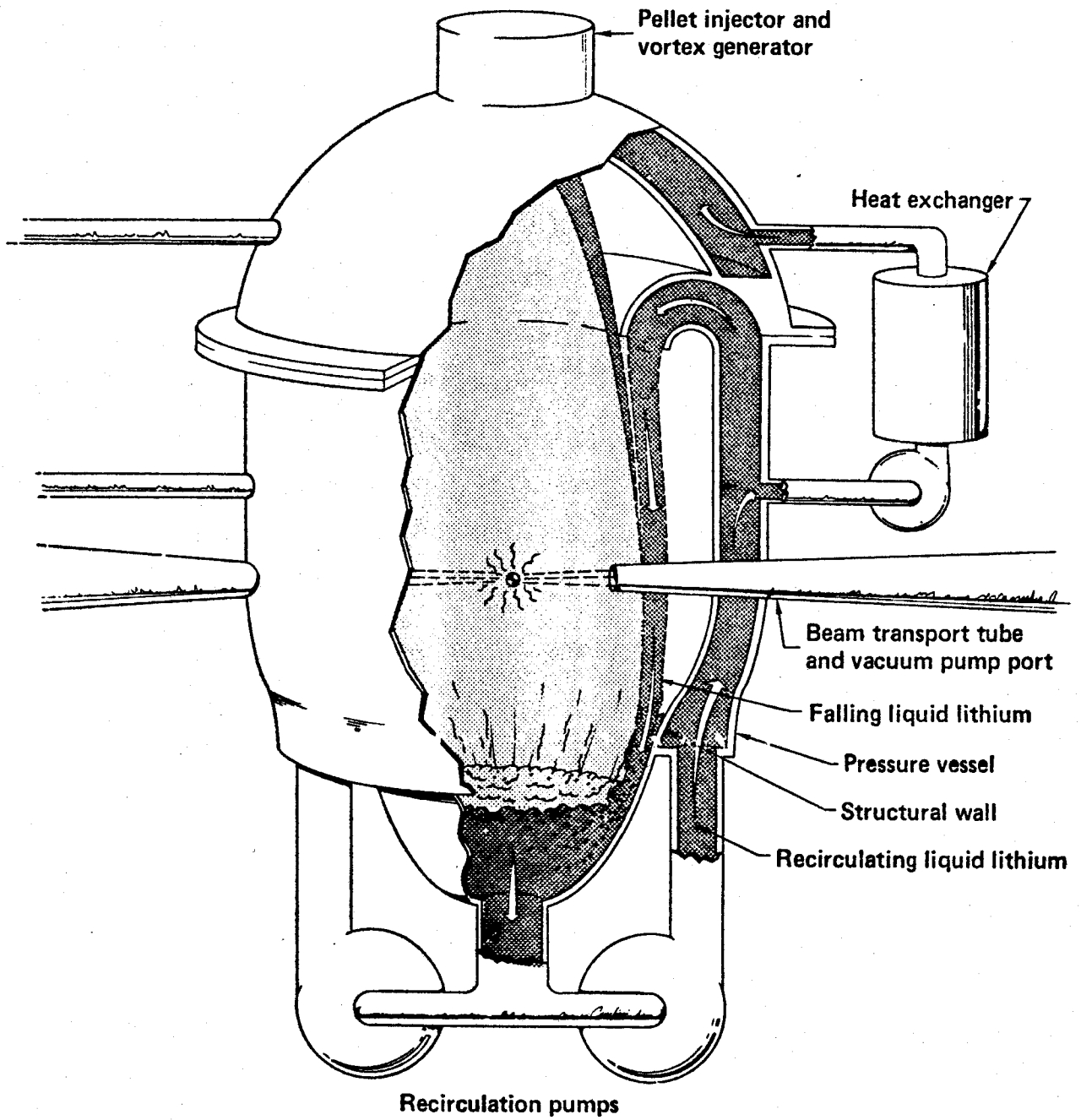

5/77

FIGURE 1-1. Laser-Fusion Reactor Showing Liquid Lithium Annular Jet

examines the dynamics of Newtonian annular jets.

The main objectives of this investigation are to identify the significant parameters affecting the dynamics of Newtonian annular jets, and to develop theoretical models for jet break-up and collapse. The dynamics of annular jets is also examined experimentally. Water is used as the working fluid in these experiments because of its ease of handling and abundance of supply. The experimental apparatus employed a sharp-edged orifice nozzle which produced an annular jet with a nearly uniform velocity distribution at the nozzle exit. This type of nozzle produces an annular jet with a radial velocity component, and closely simulates the lithium waterfall design. The non-zero radial velocity component can be attributed to the fact that the streamlines must be continuous and differentiable along their entire paths; at the nozzle exit the streamlines cannot bend abruptly around the sharp-edged orifice plates. This emphasizes the importance of studying how the nozzle design will affect the dynamics of the annular jet. Other parameters that affect the dynamics of annular jets are the Weber number, and the aspect ratio (i.e. the ratio of the inside diameter to the outside diameter).

A number of interesting phenomena were observed during the experimental part of the investigation. The sharp-edged orifice nozzle was designed such that air could be injected into the center of the jet. When air was injected at a velocity equal to the average water velocity, the annular jet was observed to break-up into hollow spherical shells of uniform size. By varying the air flow rate about its nominal value, it was possible to increase or decrease the size of the

spherical shells. This mode of jet break-up is predicted by the stability theory presented in section 3.1.

Undoubtedly, many engineering applications of this mode of jet break-up will be found. Some possible applications might include the development of an automotive carburetor which will give precise mixtures of air and fuel. Another interesting possibility is the production of hard spherical shells by forcing a molten extrudate through the nozzle and allowing it to cool as it falls. However, it should be kept in mind that this mode of jet break-up occurred only when air was forced into the center of the annular jet.

When the center of the annular jet was vented to atmospheric pressure, the jet collapsed into a solid circular jet over a length of 1 to 2 nozzle diameters. The closure distance was determined primarily by the radial velocity component of the jet, and secondarily by fluid surface tension forces. A theoretical model describing this phenomenon is presented in section 3.3.

The remainder of this thesis is organized as follows: Section 1.1 contains a literature survey of closely related experiments with solid circular jets. The experimental apparatus and test procedure are described in Chapter 2. Chapter 3 contains the derivation of theoretical models and comparison with experimental results. The conclusions and recommendations of this investigation are given in Chapter 4.

1.1 Literature Survey

The literature contains numerous investigations on the stability of solid circular jets. By definition, a solid circular jet contains

only one free surface. Savart [4], Plateau [5], and most notably Lord Rayleigh [6, 7, 8, 9] were the first to analyze the stability of solid circular jets. Rayleigh's dispersion relation has been subjected to rigorous experimental investigation. Its validity has been recently proven by Goedde and Yuen [10], Donnelly and Glaberson [11], Crane, Birch, and McCormack [12, 13]; and by older experiments performed by Merrington and Richardson [14], Tyler and Watkin [15], Tyler [16], and Smith and Moses [17].

To date, the stability of annular jets has not been examined. Annular jets differ from solid circular jets in that they have two free surfaces. They have numerous practical applications. The motivation for this investigation arose from interest in the lithium waterfall cavity design proposed for use in laser-fusion reactors by Maniscalco and Meier [1], and Powell, Lazareth, and Fillo [2].

The work presented here on the derivation of the dispersion relations for annular jets (see section 3.1) parallels that given by Rayleigh [6, 7, 8, 9] and Chandrasekhar [18], except now there are two dispersion relations corresponding to the two free surfaces of the annular jet.

Recently, several non-linear theories on the stability of solid circular jets have appeared in the literature. In particular, Wang [19], and Yuen [20] have shown that finite amplitude disturbances need to be considered to correctly predict the non-sinusoidal surface deformation of the jet. Lafrance [21], Tassoul and Aubin [22], and Nayfeh [23] have written mathematical treatises describing the non-linear theory of jet break-up. A similar analysis could be per-

formed for annular jets, but this is beyond the scope of this paper. Mention of finite amplitude disturbances is made with the intention that at some later date, if deemed useful, the non-linear theory could be developed in much the same way as was done for solid circular jets.

It should be noted that the dispersion relations derived for solid and annular jets are valid only for laminar flow conditions. However, this does not diminish the value of these results inasmuch as they can be extended to turbulent flow conditions. Phinney [24], Chen and Davis [25], Fenn and Middleman [26], Grant and Middleman [27], Miesse [28], and Lafrance [29] have used the linear theory of solid circular jets to develop empirical correlations to fit the experimental data for turbulent jets. A recent paper by Hoyt and Taylor [30] provides insight into the physical mechanisms causing break-up of turbulent jets. They have shown that the initial break-up of the jet is caused by inherent turbulence, and the interaction between the surface tension and inertial forces. Air friction is responsible for the dispersion of the jet into fine droplets. These studies are important in relation to turbulent annular jets in that one expects the same mechanisms to be present.

CHAPTER 2

EXPERIMENTAL APPARATUS AND TECHNIQUES

To aid in our understanding of the dynamics of annular jets an experimental apparatus was constructed whereby all the relevant parameters could be carefully controlled and measured during the tests. Figure 2-1 shows the complete experimental apparatus. The outer frame supports the main water reservoir eight feet above ground level. The water flows by gravity from the main reservoir through a quieting chamber to the nozzle. Located on one side of the test stand are all of the measuring instruments and controls. A Hycam high speed movie camera is mounted in front of the test stand in order to record the experimental data. This camera can be replaced with a Nikon single lens reflex camera for taking still photographs. Both cameras were used extensively to record events.

An inner frame supports the quieting chamber and nozzle assembly. The inner frame is unattached to the test stand, except for nozzle piping. This prevents any external vibrations from disrupting the nozzle flow. Surrounding the nozzle outlet are four banks of photo lights, each capable of focusing 600 watts of light on the jet. With light of this intensity it was possible to take movie pictures at a rate of 5000 frames per second on 16 mm film. At this speed, a 100 foot roll of film goes through the camera in less than one-half of a second. Clearly, this method of recording data becomes very expensive for large numbers of test cases. Therefore, a still camera was used to screen a large number of test cases, and only those cases

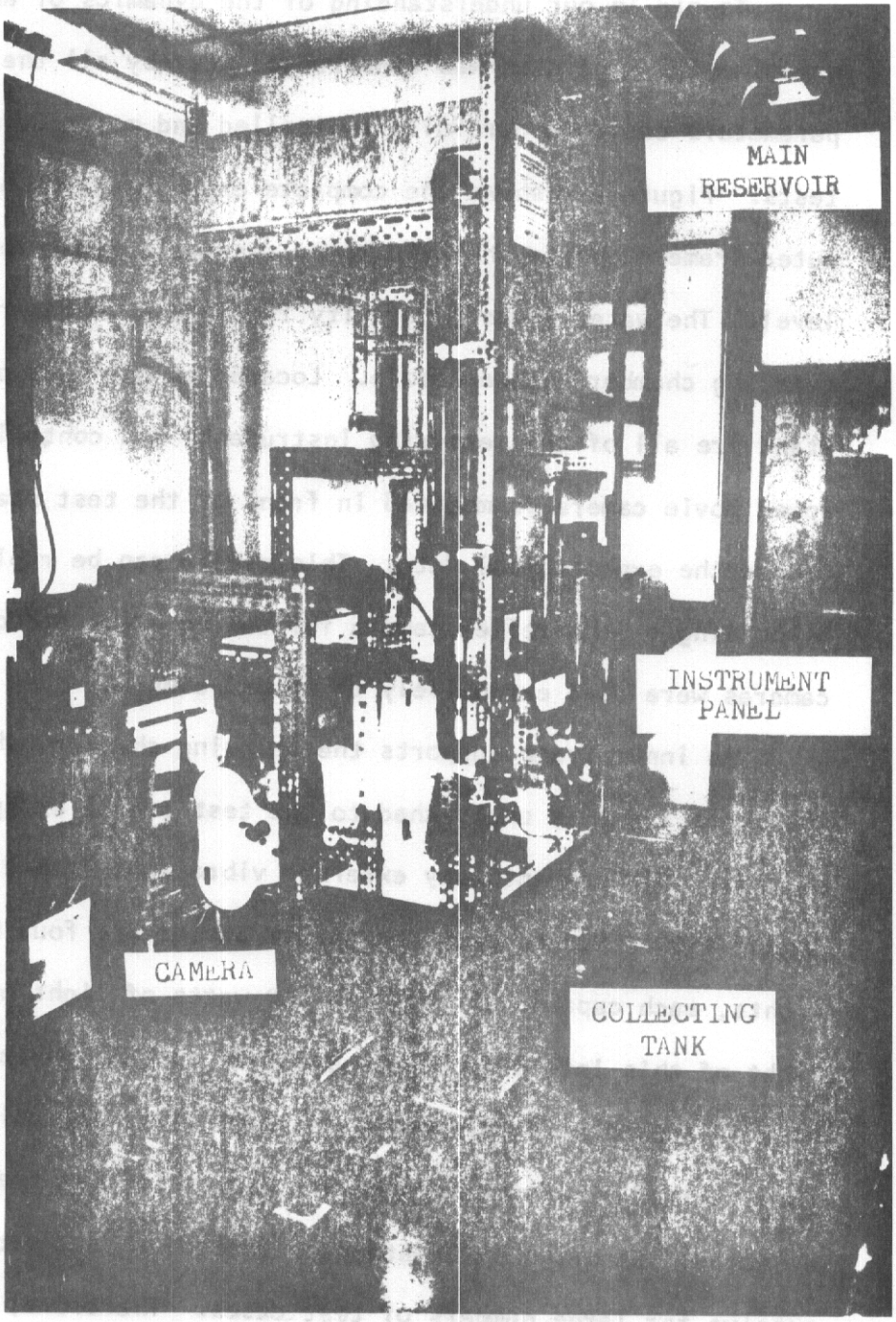

Figure 2-1. The Experimental Apparatus.

of particular interest were repeated using the movie camera to record the event. The movie helps illustrate the main features of the annular jet break-up and collapse.

2.1 The Experimental Arrangement

Figure 2.2 shows a schematic diagram of the experimental arrangement showing the principal parts and flow directions. The upper feed tank may be filled in one of two ways. If water is the working fluid, the tank is filled by opening the shut-off valve on the supply line attached to the tank. If another working fluid is desired, it may be added to the collecting tank, and then pumped up to the feed tank. Once the upper feed tank is full, a control valve is opened to start the flow to the nozzle. A rotameter placed in the feed line accurately measures the flow rate. As mentioned previously, gravity is the only driving force for fluid flow. No pumps are allowed to be running when the nozzle is operating. To get a constant pressure head, the upper feed tank was made large enough so that its level did not drop appreciably during the course of the experiment.

Before being discharged through the nozzle, the fluid enters a large quieting chamber that serves to reduce the turbulence in the system. The quieting chamber contains copper screening of 20 x 20 mesh spacing to damp out any turbulent eddies. Also, the quieting chamber is vented to the atmosphere in order to allow any air trapped in the system to escape. A sealed air line is passed through the quieting chamber and connected to the center rod of the nozzle. The center rod has a hole bored out so that air can be forced through the center of the jet. A control valve is used to adjust the air flow

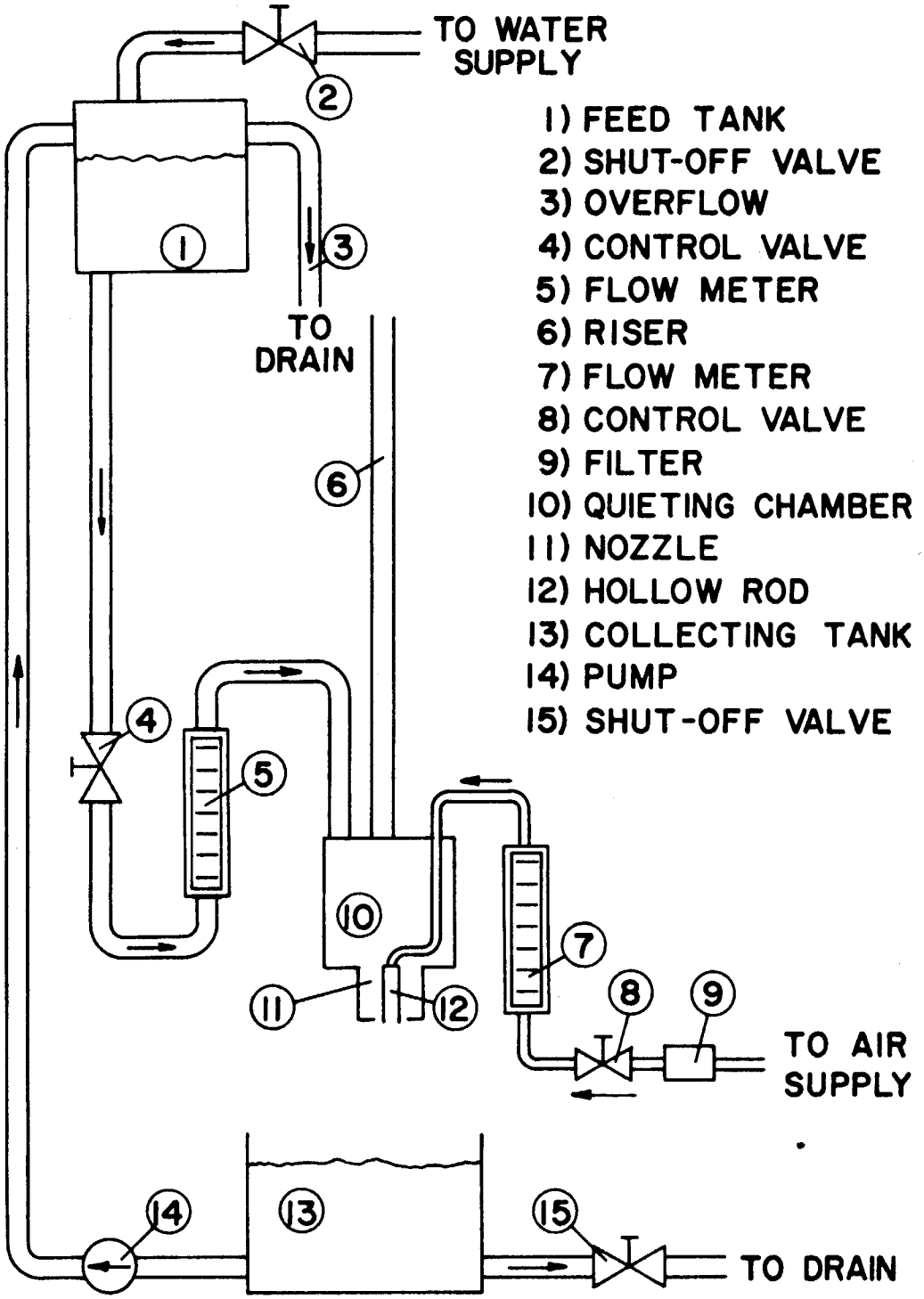

FIGURE 2-2. Sketch of Apparatus Showing the Principal Parts of the Flow System.

and a rotameter accurately measures the air flow rate. In this way, air can be injected into the center of the annular jet at a known rate. All liquid discharged from the nozzle is collected in the bottom tank, and may either be pumped back up to the feed tank, or discharged to a drain.

2.2 Nozzle Design

Figure 2-3 shows the top and side views of the sharp-edged orifice nozzle assembly. All of the nozzle components are made out of aluminum with machine tolerences held within $\pm$ 0.002 inches. The nozzle assembly was designed such that it could easily be removed from the quieting chamber by unbolting six cap screws.

Figure 2-4 shows a cross-section of the nozzle assembly revealing the principal components. The different nozzle components are designed such that they can be easily dissassembled and replaced with new components to obtain a different nozzle geometry. For instance, the bottom orifice plate is easily removed from the nozzle support structure, and can be replaced with a new orifice plate of a different diameter opening. Likewise, the center rod can be replaced with another of a different size. Nozzles with a wide range of aspect ratios (r_i/r_o) can be assembled using the same basic nozzle support structure.

An important feature of this nozzle design is the use of sharp-edged orifices for both the bottom plate and center rod. By employing this design, it was possible to produce an annular jet with a nearly uniform velocity distribution at the nozzle exit. This differs from nozzles employing concentric cylinders of sufficient

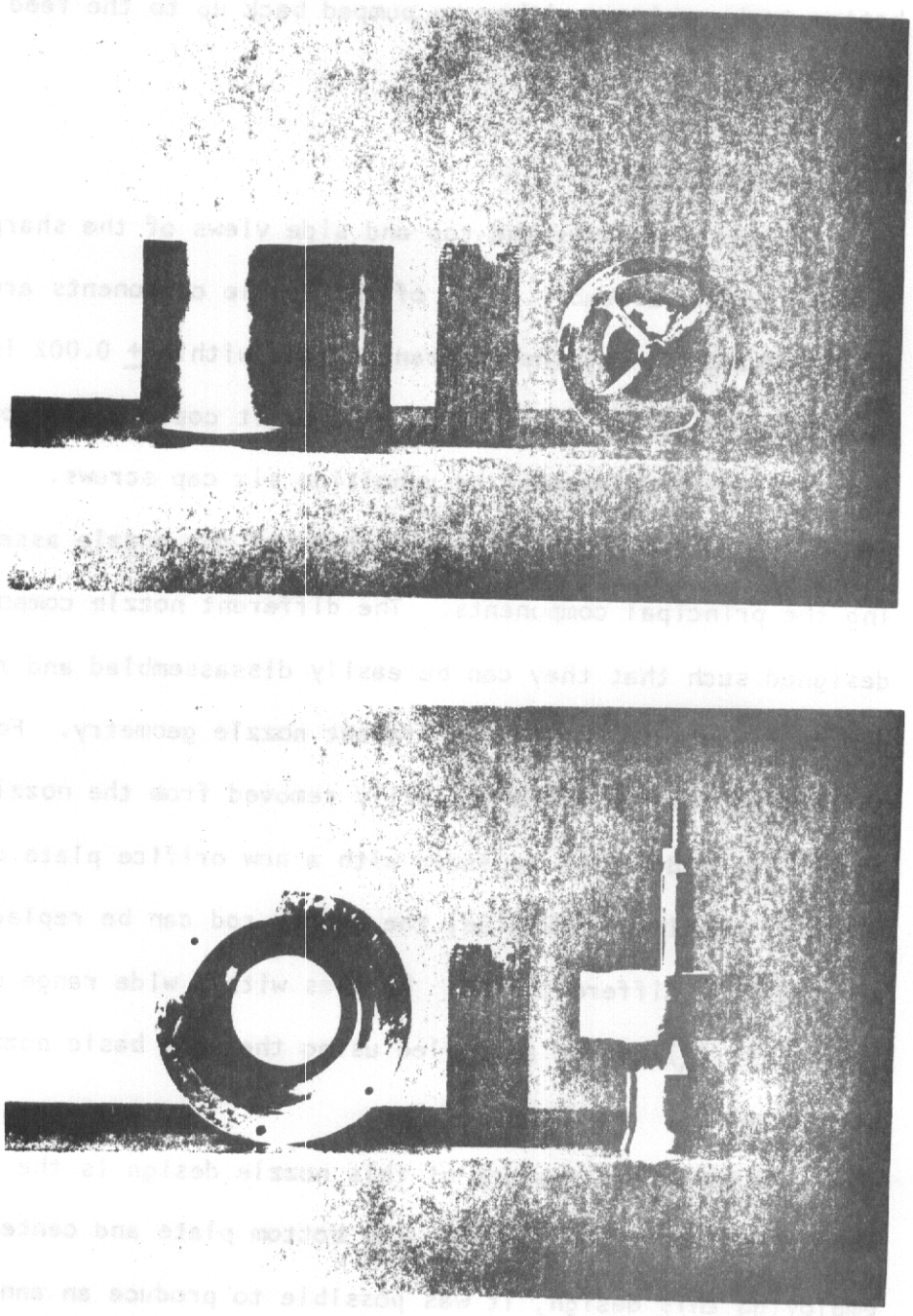

Figure 2-3. Sharp-Edged Orifice Nozzle Components.

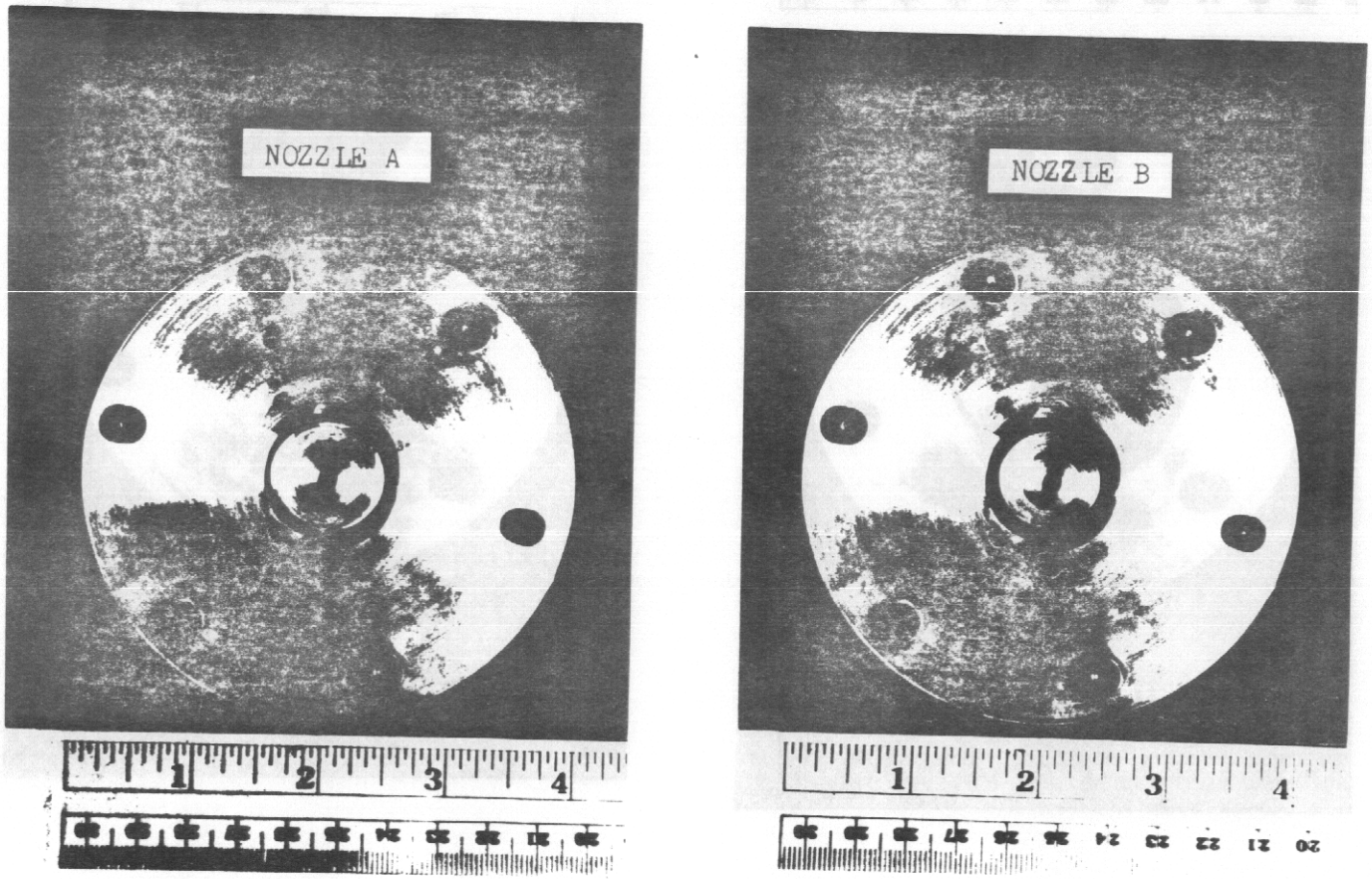

Figure 2-5. Test Nozzles A and B Showing Orifice Plate and Center Rod Arrangement.

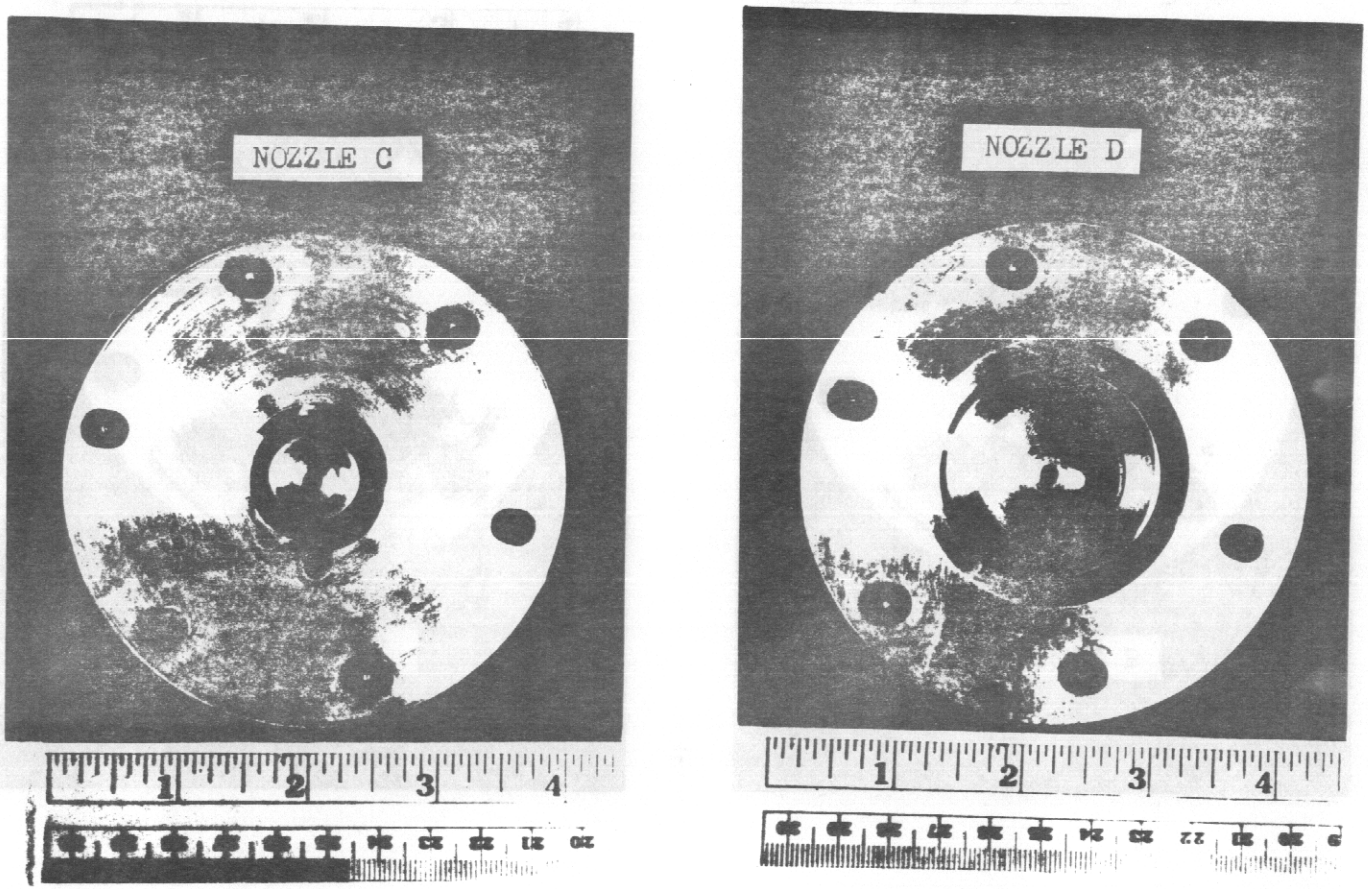

Figure 2-6. Test Nozzles C and D Showing Orifice Plate and Center Rod Arrangement.

2.3 Test Procedure

The first step in setting up the experiment is to fill the upper feed tank with the desired fluid. It takes about 5 minutes to fully charge the feed tank. The test begins by opening the control valve on the supply line to the nozzle. At first the valve is opened up completely to allow the quieting chamber and nozzle piping to be filled with liquid. It takes a few minutes to remove all of the air trapped in the system. During this time the air flow rate to the center rod of the nozzle is adjusted to the desired setting. The control valve for the liquid flow to the nozzle is then adjusted to the desired flow rate. Once this is completed, steady-state conditions are established in less than one minute.

Next, the liquid and air flow rates are recorded, and a photograph is taken of the annular jet. While the data is being recorded, all pumps and mechanical devices are turned-off in order to prevent any external vibrations from affecting the annular jet. For each test case, the entire procedure from set-up to recording the data takes about 15 minutes. Over 100 test cases were recorded on film. The main parameters for these tests are listed in Table 2-II.

TABLE 2-II. Parameters Recorded During Testing

	Measured	Calculated
Nozzle Characteristics		
Outside Diameter	X	
Inside Diameter	X	
Aspect Ratio		X
Flow Characteristics		
Water Flow Rate	X	
Air Flow Rate	X	
Water Velocity		X
Air Velocity		X
Water Temperature	X	
Weber Number		X
Photographic Analysis		
Scanner Conversion Factor	X	
Outside Surface (r = f(z))	X	

CHAPTER 3

THEORY AND COMPARISON WITH EXPERIMENTAL RESULTS

In this chapter we present theoretical models to predict: (1.) The modes of jet break-up, (2.) The effect of nozzle design on jet dynamics, and (3.) The profiles of annular jets without air injection. In each section experimental results are presented and compared with the theoretical models.

3.1 Modes of Jet Break-up

In this section we investigate the stability of an annular jet when subjected to an infinitesmal displacement from its equilibrium position. If the perturbations are damped out in time we say the system is stable; but if the perturbations are amplified in time, and eventually cause the jet to break-up, we say the system is unstable. We begin the analysis by considering the section of the annular jet shown in Fig. 3-1. The dashed lines represent the deformed surfaces, and are described by the equations

$$\omega_1 = r_1 + \epsilon_1 \exp\left[i(k_1 z + m_1 \theta + \phi)\right] \qquad (3.1\ a)$$

and,

$$\omega_2 = r_2 + \epsilon_2 \exp\left[i(k_2 z + m_2 \theta)\right] \qquad (3.1\ b)$$

In these equations k_1, k_2, m_1, and m_2 are wave numbers; ϵ_1 and ϵ_2 are the amplitudes of the perturbations; and ϕ is an arbitrary phase

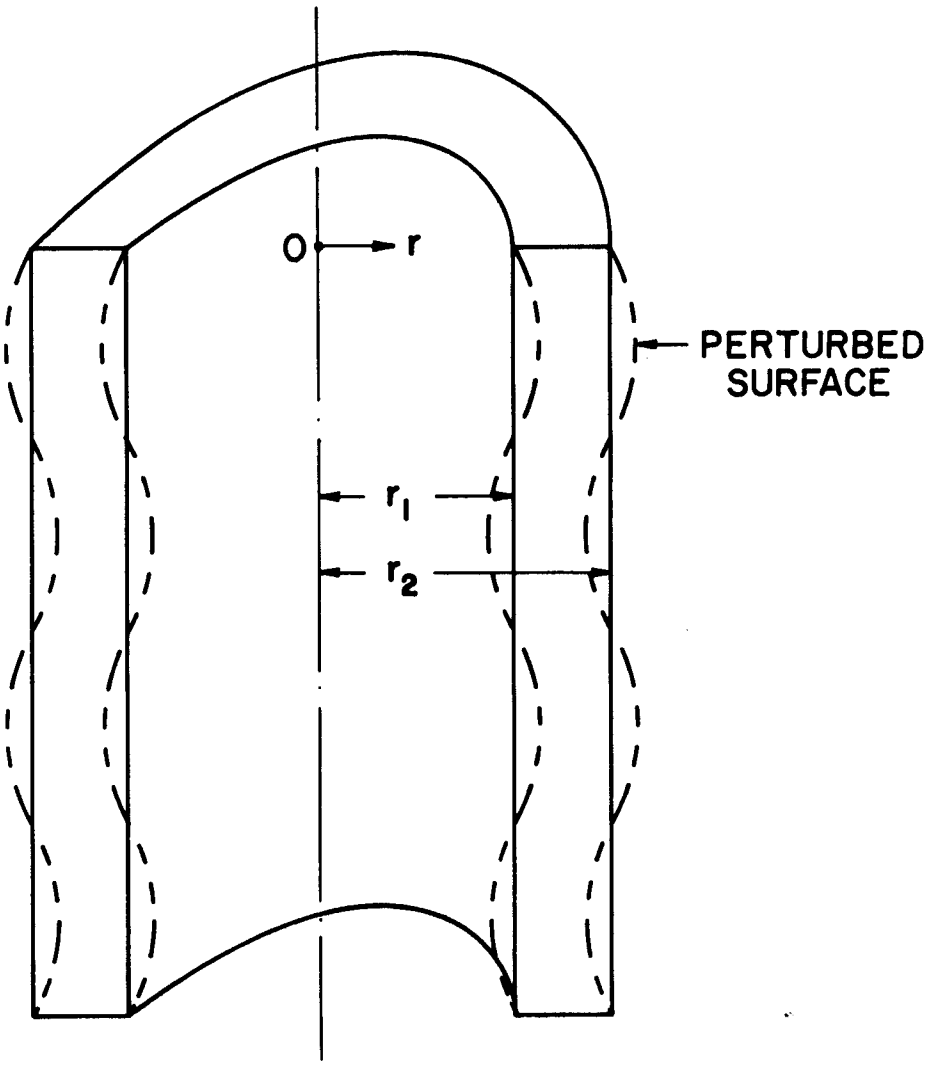

FIGURE 3-1. Cross Section of Annular Jet Showing Perturbed Surfaces.

angle between the waves at the free surfaces. All possible frequencies at which the surface can be disturbed have been included in the analysis by allowing all the wave numbers to assume any integer value from the set: $\{0,1,2,3,....\infty\}$. The set of wave numbers which lead to an unstable equilibrium are called the dispersion wave numbers, and are defined by a dispersion relation. Subsequently, we will derive the dispersion relation for annular jets.

The linear perturbation equations are:

$$\frac{\partial \vec{u}}{\partial t} = -\text{grad}\,\pi \tag{3.2}$$

$$\text{div}\,\vec{u} = 0 \tag{3.3}$$

$$\pi = \frac{\delta p}{\rho} \tag{3.4}$$

Here we have deliberately neglected the terms involving the fluid viscosity. This simplifies the mathematical analysis, and still provides us with the information we want.

By taking the divergence of both sides of Eqn. 3.2, and using continuity relationship, Eqn. 3.3, we obtain Laplace's equations in the form

$$\nabla^2\pi = 0 \tag{3.5}$$

This equation is most easily solved for the case of an annular jet by making use of the principle of superposition. The problem is split into two separate problems by defining

$$\eta = \eta_1 + \eta_2 \tag{3.6}$$

We define the η_1 problem such that it contains only the perturbation at the ω_1 surface, and we define the η_2 problem such that it contains only the perturbation at the ω_2 surface. Boundary conditions for the η_1 and η_2 problems are obtained by recognizing that

$$P_0 + \delta p = \sigma \left(\frac{1}{R_1} + \frac{1}{R_2} \right) \tag{3.7}$$

where R_1 and R_2 are the principle radii of curvature at the surface. For the unperturbed annular wall we know

$$P_{01} = \frac{\sigma}{r_1} \tag{3.8 a}$$

$$P_{02} = \frac{\sigma}{r_2} \tag{3.8 b}$$

Equation 3.7 is solved for δp_1 or δp_2 using either Eqn. 3.8 a or 3.8 b, to give the boundary conditions for the η_1 problem as

$$\eta_1 (r_2) = 0 \tag{3.9 a}$$

$$\eta_1(\omega_1) = \frac{\sigma}{r_1^2 \rho}\left(1 - m_1^2 - x_1^2\right)\epsilon_1 \exp\left[i(k_1 z + m_1 \theta + \phi)\right] \qquad (3.9\ b)$$

and for the η_2 problem the boundary conditions are

$$\eta_2(r_1) = 0 \qquad (3.10\ a)$$

$$\eta_2(\omega_2) = \frac{\sigma}{r_2^2 \rho}\left(1 - m_2^2 - x_2^2\right)\epsilon_2 \exp\left[i(k_2 z + m_2 \theta)\right] \qquad (3.10\ b)$$

By assuming solutions of a form consistent with the equations of the deformed boundaries, such as

$$\eta_1 = \Omega_1(r)\,\epsilon_1 \exp\left[i(k_1 z + m_1 \theta + \phi)\right] \qquad (3.11\ a)$$

$$\eta_2 = \Omega_2(r)\,\epsilon_2 \exp\left[i(k_2 z + m_2 \theta)\right] \qquad (3.11\ b)$$

we obtain two Bessel equations which are solved explicitly to obtain the functions $\Omega_1(r)$ and $\Omega_2(r)$. Complete solutions to the η_1 and η_2 problems are obtained by substituting $\Omega_1(r)$ and $\Omega_2(r)$ back into Eqn. 3.11 a and Eqn. 3.11 b, respectively. The solution for π, as defined by Eqn. 3.6, is given in Fig. 3-2. In Eqn. 3.12, $I_m(x)$ is the modified Bessel function of the first kind of order m, and $K_m(x)$ is the modified Bessel function of the second kind of order m.

We can now examine the growth or decay of the perturbations by defining the wave amplitudes as

$$\pi = \left[\frac{K_{m_1}\left(\frac{x_1}{\alpha}\right) I_{m_1}(k_1 r) - I_{m_1}\left(\frac{x_1}{\alpha}\right) K_{m_1}(k_1 r)}{I_{m_1}\left(\frac{x_1}{\alpha}\right) K_{m_1}(x_1) - I_{m_1}(x_1) K_{m_1}\left(\frac{x_1}{\alpha}\right)}\right] \frac{\sigma}{r_1^2 \rho} (1 - m_1^2 - x_1^2) \epsilon_1 \exp\left[i(k_1 z + m_1 \theta + \phi)\right]$$

$$+ \left[\frac{K_{m_2}(\alpha x_2) I_{m_2}(k_2 r) - I_{m_2}(\alpha x_2) K_{m_2}(k_2 r)}{I_{m_2}(x_2) K_{m_2}(\alpha x_2) - K_{m_2}(x_2) I_{m_2}(\alpha x_2)}\right] \frac{\sigma}{r_2^2 \rho} (1 - m_2^2 - x_2^2) \epsilon_2 \exp\left[i(k_2 z + m_2 \theta)\right] \qquad (3.12)$$

FIGURE 3-2. Equation 3.12 for the Perturbed Pressure.

$$\epsilon_1 = \epsilon \exp[\nu_1 t] \quad \text{, and} \tag{3.13 a}$$

$$\epsilon_2 = \epsilon \exp[\nu_2 t] \tag{3.13 b}$$

When the amplification factors, ν_1 and ν_2, are negative, the infinitesmal perturbations are damped out in time, and the system is stable. However, when the amplification factors are positive, the perturbation amplitudes grow in time, and we have an unstable mode. To obtain the dispersion relation for the unstable modes, we begin by substituting Eqn. 3.12 into Eqn. 3.2 to get an expression for the perturbation velocities. In particular, the perturbation velocity in the radial direction is given in Fig. 3-3.

The perturbation velocities must also be consistent with the perturbation equations of the free surfaces given by Eqns. 3-1 a and 3-1 b. Differentiating these equations with respect to time yields,

$$u_{\omega_1} = \nu_1 \epsilon \exp[i(k_1 z + m_1 \theta + \phi) + \nu_1 t] \tag{3.15}$$

$$u_{\omega_2} = \nu_2 \epsilon \exp[i(k_2 z + m_2 \theta) + \nu_2 t] \tag{3.16}$$

Equating Eqn. 3.15 with Eqn. 3.14 at the boundary $r = r_1$ yields the dispersion relation given in Fig. 3-4. Likewise, the dispersion relation for the free surface at $r = r_2$ is obtained by equating Eqn. 3.16 to Eqn. 3.14. Figure 3-5 gives the dispersion relation for the

$$u_r = \left[\frac{K_{m_1}\left(\frac{x_1}{\alpha}\right) I_{m_1+1}(k_1 r) - I_{m_1}\left(\frac{x_1}{\alpha}\right) K_{m_1+1}(k_1 r)}{I_{m_1}\left(\frac{x_1}{\alpha}\right) K_{m_1}(x_1) - I_{m_1}(x_1) K_{m_1}\left(\frac{x_1}{\alpha}\right)} \right] \frac{\sigma}{r_1^3 \rho} (1 - m_1^2 - x_1^2) \frac{x_1 \epsilon}{\nu_1} \exp\left[i(k_1 z + m_1 \theta + \phi) + \nu_1 t \right]$$

$$+ \left[\frac{K_{m_2}(\alpha x_2) I_{m_2+1}(x_2) - I_{m_2}(\alpha x_2) K_{m_2+1}(x_2)}{I_{m_2}(x_2) K_{m_2}(\alpha x_2) - I_{m_2}(\alpha x_2) K_{m_2}(x_2)} \right] \frac{\sigma}{r_2^3 \rho} (1 - m_2 - x_2^2) \frac{x_2 \epsilon}{\nu_2} \exp\left[i(k_2 z + m_2 \theta) + \nu_2 t \right] \qquad (3.14)$$

FIGURE 3-3. Equation 3.14 for the Perturbation Velocities.

$$\nu_1^2 = \left[\frac{K_{m_1}\left(\frac{\chi_1}{\alpha}\right) I_{m_1+1}(\chi_1) - I_{m_1}\left(\frac{\chi_1}{\alpha}\right) K_{m_1+1}(\chi_1)}{I_{m_1}\left(\frac{\chi_1}{\alpha}\right) K_{m_1}(\chi_1) - I_{m_1}(\chi_1) K_{m_1}\left(\frac{\chi_1}{\alpha}\right)} \right] \frac{\sigma}{r_1^3 \rho} (1 - m_1^2 - \chi_1^2) \chi_1$$

$$+ \left[\frac{K_{m_2}(\alpha\chi_2) I_{m_2+1}(\alpha\chi_2) - I_{m_2}(\alpha\chi_2) K_{m_2+1}(\alpha\chi_2)}{I_{m_2}(\chi_2) K_{m_2}(\alpha\chi_2) - I_{m_2}(\alpha\chi_2) K_{m_2}(\chi_2)} \right] \frac{\sigma}{r_2^3 \rho} (1 - m_2^2 - \chi_2^2) \frac{\chi_2 \nu_1}{\nu_2} \exp\left[i\left((k_2 - k_1) z + (m_2 - m_1)\theta - \beta \right) + (\nu_2 - \nu_1) t \right] \quad (3.17)$$

FIGURE 3-4. Dispersion Relation for the Free Surface at r_1.

$$\nu_2^2 = \left[\frac{K_{m_1}\left(\frac{\chi_1}{\alpha\epsilon}\right) I_{m_1+1}\left(\frac{\chi_1}{\alpha\epsilon}\right) - I_{m_1}\left(\frac{\chi_1}{\alpha\epsilon}\right) K_{m_1+1}\left(\frac{\chi_1}{\alpha\epsilon}\right)}{I_{m_1}\left(\frac{\chi_1}{\alpha\epsilon}\right) K_{m_1}(\chi_1) - I_{m_1}(\chi_1) K_{m_1}\left(\frac{\chi_1}{\alpha\epsilon}\right)}\right] \frac{\sigma}{r_1^3\rho} (1-m_1^2-\chi_1^2) \frac{\chi_1 \nu_1}{\nu_2} \exp\left[i\left((k_1-k_2)z + (m_1-m_2)\theta + \phi\right) + (\nu_1-\nu_2)t\right]$$

$$+ \left[\frac{K_{m_2}(\alpha\chi_2) I_{m_2+1}(\chi_2) - I_{m_2}(\alpha\chi_2) K_{m_2+1}(\chi_2)}{I_{m_2}(\chi_2) K_{m_2}(\alpha\chi_2) - I_{m_2}(\alpha\chi_2) K_{m_2}(\chi_2)}\right] \frac{\sigma}{r_2^3\rho} (1-m_2^2-\chi_2^2)\chi_2 \qquad (3.18)$$

FIGURE 3-5. Dispersion Relation for the Free Surface at r_2.

surface at $r = r_2$.

Equations 3.17 and 3.18 constitute a set of equations which must be solved simultaneously to obtain values of the amplification factors. However, we need not solve these equations completely to determine the mode by which the annular jet will break-up. Notice that the annular jet is unstable only for positive values of ν_1 and ν_2. It can be shown that the Bessel function terms within brackets always reduce to a positive number for any given value of α and x_1 and x_2. By inspection we conclude that unstable modes can only exist for $m_1 = m_2 = 0$, and for $0 < x_1 < 1$ and $0 < x_2 < 1$. Any other choice of m_1 and m_2, or x_1 and x_2 will give negative amplification factors and, hence, stable modes. In effect, this says the annular jet is unstable for axisymmetric disturbances with wavelengths exceeding the circumference of the inside surface at $r = r_1$; and, likewise, at $r = r_2$ the annular jet is unstable for axisymmetric disturbances with wavelengths exceeding the circumference of the outside surface. Also, for all purely non-axisymmetric deformations, i.e. $m_1 \neq 0$ and $m_2 \neq 0$, the annular jet is stable.

Furthermore, it can be shown that the dispersion relations have a maximum positive value when $k_1 = k_2$, and the phase angle, ϕ, between the perturbations is zero. In other words, the dispersion relations are maximized when the deformations at each free surface have the same wavelength and are in phase. This is exactly the case shown in Fig. 3-1. One expects the dispersion mode with the largest positive value to dominate the break-up of the jet. Therefore, we can expect the annular jet to eventually break-up into spherical shells. The

size and thickness of the spherical shells will depend on the wavelength of the disturbance and the initial thickness of the annular jet. If there is a gas on the inside of the annular jet, the spherical shells will collapse until the forces due to surface tension in the fluid balance the gas pressure. This suggests an interesting application. By injecting a gas into the center of the annular jet, we should be able to control the size of the spherical shells. Indeed, when we actually performed the experiment this phenomenon was observed.

Figure 3-6 shows an annular jet breaking up into hollow spherical shells. The experimental conditions for this test case are given in Table 3-1. In this case, the air velocity in the center of the annular jet was greater than the average water velocity. This mode of jet break-up was observed only when the air velocity approached the average water velocity. Physically, this can be explained because the size of the spherical shells is determined by requiring the forces arising from surface tension to balance the air pressure inside the jet. For instance, if the annular jet was ejected into a vacuum, one would expect the spherical shells to collapse completely because there would not be any gas on the inside to counterbalance surface tension forces. Indeed, this was found to be the case when the center of the jet was vented to the atmosphere so that the pressure on the inside and the pressure on the outside were exactly equal (see section 3.3).

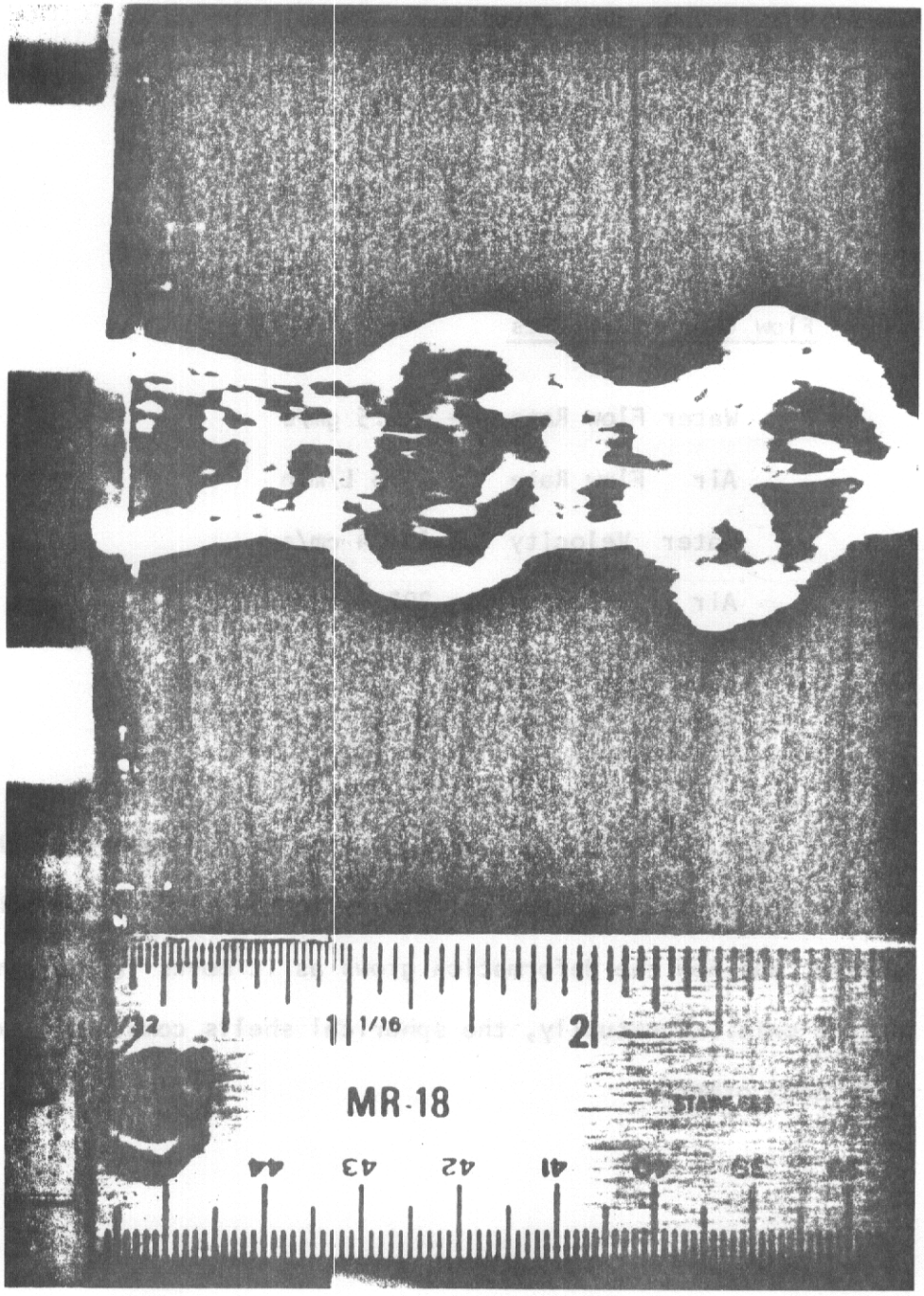

Figure 3-6. Annular Jet Breaking Up Into Hollow Spherical Shells.

TABLE 3-1. Experimental Conditions For A Test Case

Nozzle Characteristics

Outside Diameter = 1.000

Inside Diameter = 0.700

Aspect Ratio = 0.700

Flow Characteristics

Water Flow Rate = 442.5 gm/s

Air Flow Rate = 43.6 L/min

Water Velocity = 171.4 cm/s

Air Velocity = 292.7 cm/s

Water Temperature = 13.0°C

Weber Number = 7.73

Figure 3-7 shows a wide angle view of the spherical shell mode of jet break-up. Note the uniformity in the size of the spherical shells, and how the deformation grows as it moves farther from the nozzle exit. Eventually, the spherical shells completely separate from each other.

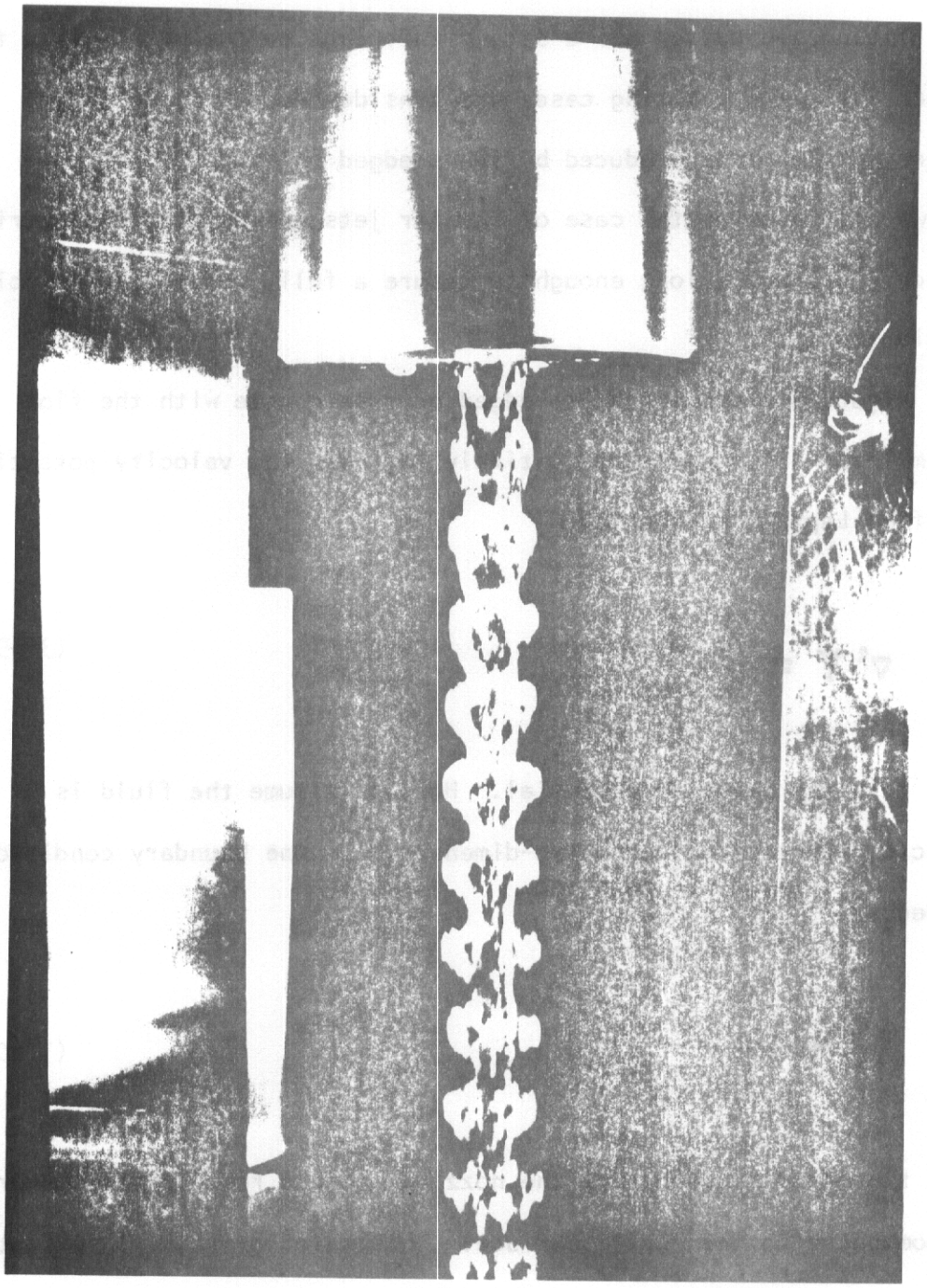

Figure 3-7. Wide Angle View of Annular Jet Breaking Up Into Hollow Spherical Shells.

3.2 Effect of Nozzle Design on Jet Dynamics

The nozzle design has a strong influence on the dynamics of the annular jet. Two limiting cases are considered. First we will examine annular jets produced by sharp-edged orifice nozzles, and then we will examine the case of annular jets produced by concentric cylinders which are long enough to insure a fully developed velocity distribution.

Figure 3-8 shows a sharp-edged orifice nozzle with the flow streamlines. If the flow is entirely laminar, the velocity potential satisfies Laplace's equation,

$$\nabla^2 \Psi = 0 \tag{3.19}$$

where Ψ is the velocity potential. Here we assume the fluid is inviscid, irrotational, and two-dimensional. One boundary condition we need is

$$\frac{\partial \Psi}{\partial n} = 0 \tag{3.20}$$

along the inside surfaces of the nozzle. Here n represents the normal component to the nozzle surface. This relation says, in effect, that fluid cannot flow into or out of the surface of the nozzle. The other boundary condition says that the velocity is constant along the streamline at the nozzle surface, or

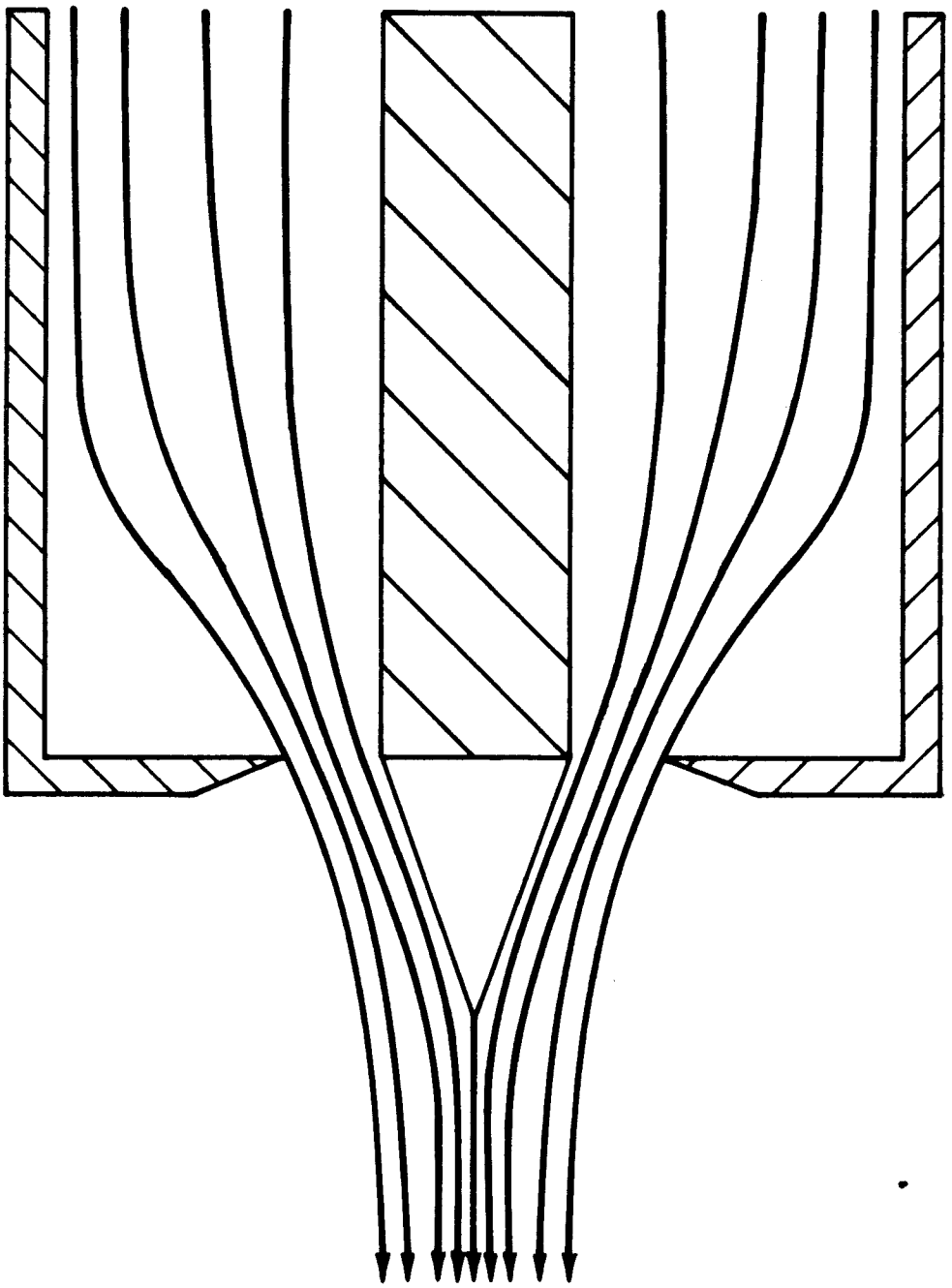

FIGURE 3-8. Sharp-Edged Orifice Nozzle With Flow Streamlines.

$$\nabla \Psi = \text{constant} \tag{3.21}$$

Indeed, this last boundary condition is somewhat artificial in that we usually require the velocity to be zero at a fixed surface. However, we are only interested in the shape of the jet as it flows from the nozzle, and the success of this method in determining the contraction coefficient for solid circular jets suggests that it might be of value for annular jets. Using the method developed by Helmholtz, conformal transformations will yield the equations for the shape of the free surfaces of the jet. The details of this procedure were not carried out due to time limitations, but the expected results can be inferred from the streamlines drawn in Fig. 3-8.

The slope of the streamlines at the nozzle exit in Fig. 3-8 show that the annular jet possesses a radial velocity component. Since the streamlines must necessarily be continuous and differentiable along their entire path, the streamline on the inside surface must have a finite slope at the nozzle exit, i.e.

$$\xi = \left.\frac{dr}{dz}\right|_{z=0} \neq 0 \tag{3.22}$$

Figure 3-9 shows an actual photograph of an annular jet. Table 3-II lists the experimental conditions for this test case. Although one can only see the outside surface on the photograph, the

thickness of this jet is 0.050 inches and to a good approximation the slope of the outside surface is equal to the slope of the inside surface at the nozzle exit. After taking measurements on a large number of photographs, the streamline slope at the nozzle exit was plotted as a function of the aspect ratio (r_i/r_o). This is shown in Fig. 3-10. The slope of the streamline at the nozzle exit can be taken as approximately constant with respect to the Weber number and the aspect ratio; its value is

$$\xi = \left.\frac{dr}{dz}\right|_{z=0} = 0.35 \tag{3.23}$$

TABLE 3-II Experimental Conditions for Test Case Shown in Fig. 3-9

Nozzle Characteristics

Outside Diameter = 1.800

Inside Diameter = 1.700

Aspect Ratio = 0.944

Flow Characteristics

Water Flow Rate = 590.0 gm/s

Air Flow Rate = vented to atmosphere

Water Velocity = 333.0 cm/s

Air Velocity = approximately zero

Water Temperature = 13.0°C

Weber Number = 8.7

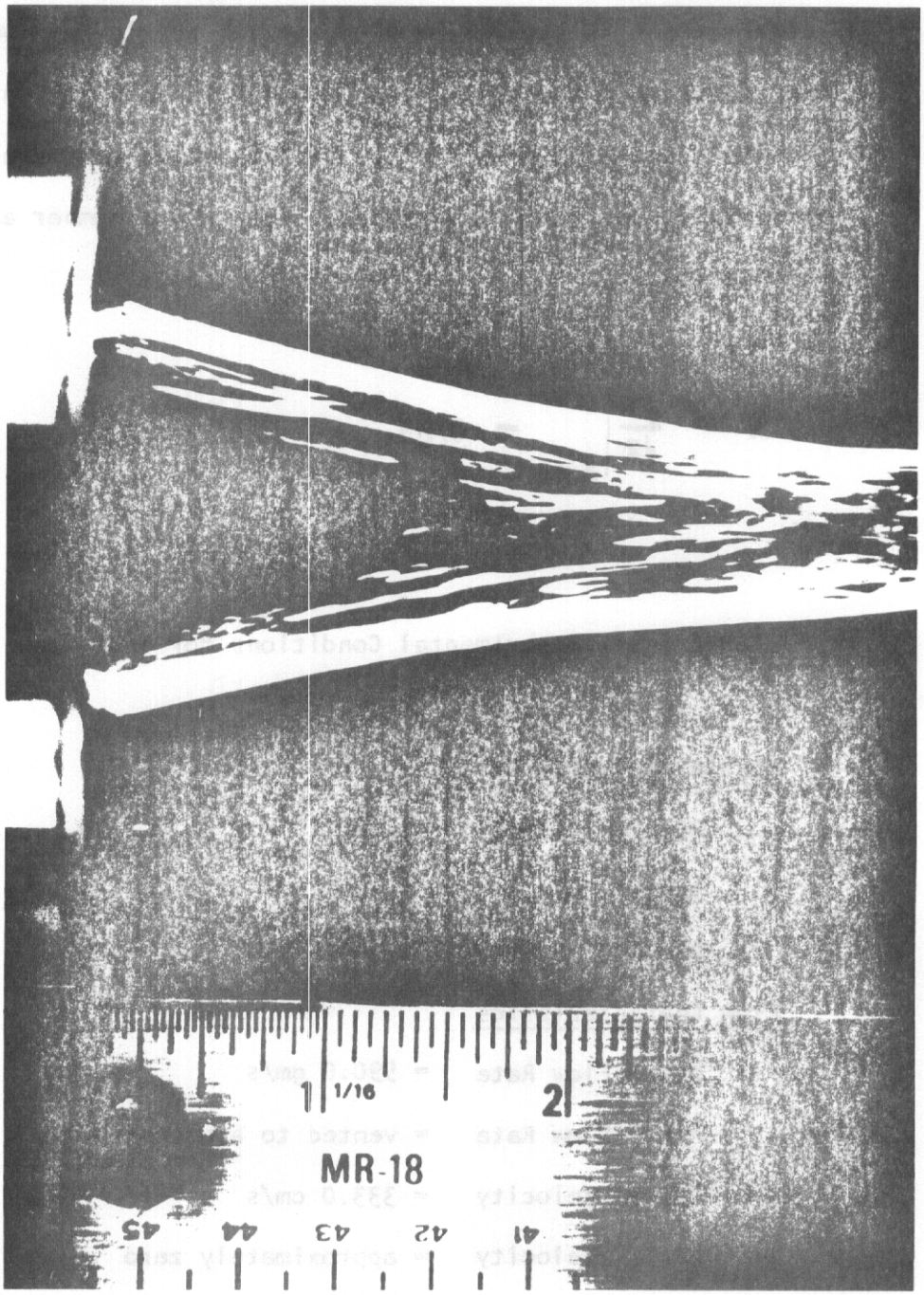

Figure 3-9. Annular Jet Showing Slope of Streamline at Nozzle Exit.

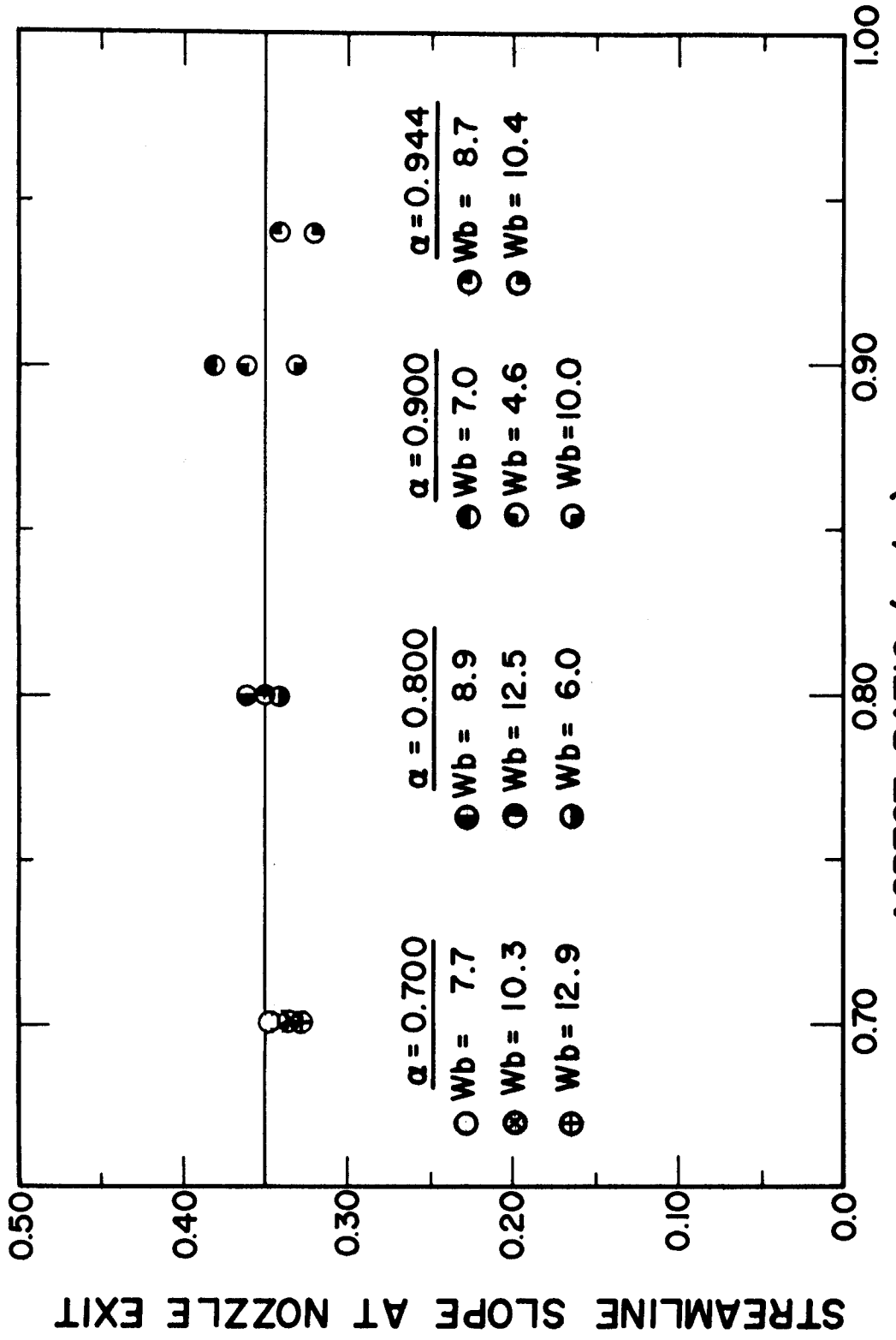

Figure 3-10. Streamline Slope at Nozzle Exit.

Another nozzle geometry to be examined is that of an annular jet produced by flow between two concentric cylinders which are sufficiently long to insure a fully developed velocity distribution. The experimental results for this type of nozzle have not been completed at the time of this writing. Mention of the concentric cylinder nozzle is made with the intent of demonstrating how another type of nozzle might affect the shape of an annular jet. Some insight into the expected behavior of this type of annular jet can be obtained through the study of solid circular jets.

In solid circular jets ejected from tubes long enough to insure a fully developed velocity profile it has been found experimentally by Middleman and Gavis [31] that for Re > 16 the jets contract. These results can be explained by using macroscopic balances. Bird [32] presents a theory which is valid for both Newtonian and non-Newtonian fluids. The contraction is due to the relaxation of the velocity profile after leaving the nozzle. As the surface shear tends to vanish the fluid at the surface accelerates while at the same time the fluid in the center decelerates. The overall effect is that the jet contracts but still maintains a constant flow rate. We expect a similar phenomenon to occur for annular jets ejected from concentric cylinder nozzles, and the methods developed previously can be extended to cover this case. At the present time we are working on both the theoretical and experimental aspects of this problem.

3.3 Profiles of Annular Jets Without Air Injection

For the case where air is not injected into the center of the annulus, but rather it is vented to the atmosphere, the pressure inside the annulus is equal to the pressure outside the annulus. Thus, the only force acting on the jet in the radial direction is that arising from surface tension of the fluid at the inside and outside surfaces. For a free surface, the pressure due to surface tension is given by

$$P = \sigma \left(\frac{1}{R_1} + \frac{1}{R_2} \right) \tag{3.24}$$

where R_1 and R_2 are the principal radii of curvature of the free surface. For annular jets, the principal radii of curvature are

$$\frac{1}{R_1} = \frac{1}{r} \tag{3.25}$$

$$\frac{1}{R_2} = \frac{\frac{d^2 r}{dz^2}}{\left[1 + \left(\frac{dr}{dz} \right)^2 \right]^{3/2}} \tag{3.26}$$

We now assume that the fluid velocity in the z-direction is sufficiently large so that for short distances from the nozzle exit gravity effects can be ignored. We also assume that the principal radius of curvature in the r-z plane is very much greater than the principal radius of curvature in the r-θ plane. The equations

of motion for the inside surface of the annular jet then reduce to the form:

$$\frac{d^2 r_i}{dt^2} + \frac{4\sigma}{\rho\left[r_o^2 - r_i^2\right]} = 0 \tag{3.27}$$

$$\frac{dz}{dt} = v_z \tag{3.28}$$

Eliminating the time dependence between these equations leaves us with one equation to solve, namely,

$$\frac{d^2 r}{dz^2} + \frac{4}{Wb^2\left(r_i + r_o\right)} = 0 \tag{3.29}$$

where the Weber number is defined as

$$Wb = v_z\sqrt{\frac{\rho X}{\sigma}} \tag{3.30}$$

Equation 3.29 is subject to the boundary condition

$$r_1 = r_l \tag{3.31}$$

at the nozzle exit, z = 0, and the other boundary condition is that the slope of the streamline at the nozzle exit is some finite

number. We may write this boundary condition as

$$\left.\frac{dr}{dz}\right|_{z=0} = \xi \tag{3.32}$$

The parameter ξ gives the effect of the nozzle design on the dynamics of the annular jet as discussed in Section 3.2. For sharp-edged orifice nozzles, ξ has a constant value of 0.35.

The differential equation defined by Eqn. 3.27 is solved subject to the boundary conditions given by Eqns. 3.31 and 3.32. The equation for the inside surface is

$$\psi_1 = \alpha - \xi\zeta - \left(\frac{4}{We^2(1+\alpha)}\right)\zeta^2 \tag{3.33}$$

where the dimensionless variables are defined as

$$\psi_1 = \frac{r_1}{r_0} \tag{3.34}$$

$$\zeta = \frac{z}{r_0} \tag{3.35}$$

Using the equation of continuity and Eqn. 3.33, the equation for the outside surface becomes

$$\psi_2 = \left[1 + \left(\frac{16}{We^4(1+\alpha)^2}\right)\zeta^4 + \left(\frac{8\xi}{We^2(1+\alpha)}\right)\zeta^3 + \left(\xi^2 - \frac{8\alpha}{We^2(1+\alpha)}\right)\zeta^2 - (2\alpha\xi)\zeta\right]^{1/2} \tag{3.36}$$

The dimensionless variable ψ_2 is given by

$$\psi_2 = \frac{r_2}{r_0} \tag{3.37}$$

The profile of the outside surface of the annular jet as given by Eqn. 3.36 is compared with measurements taken from photographs of various test cases. Figure 3-11 shows a photograph of an annular jet produced by nozzle A. Table 3-III lists the experimental conditions for this test case. This jet has a thickness of 0.050 inches, and it collapses rather quickly to a solid circular jet. Jet dimensions taken from the photograph are plotted along with the theoretical results in Fig. 3-12. Agreement between theory and experiment is excellent.

TABLE 3-III. Experimental Conditions For Nozzle A

Nozzle Characteristics

Outside Diameter = 1.000

Inside Diameter = 0.900

Aspect Ratio = 0.900

Flow Characteristics

Water Flow Rate = 368.8 gm/s

Air Flow Rate = vented to atmosphere

Water Velocity = 383.4 cm/s

Air Velocity = approximately zero

Water Temperature = 13.0°C

Weber Number = 10.0

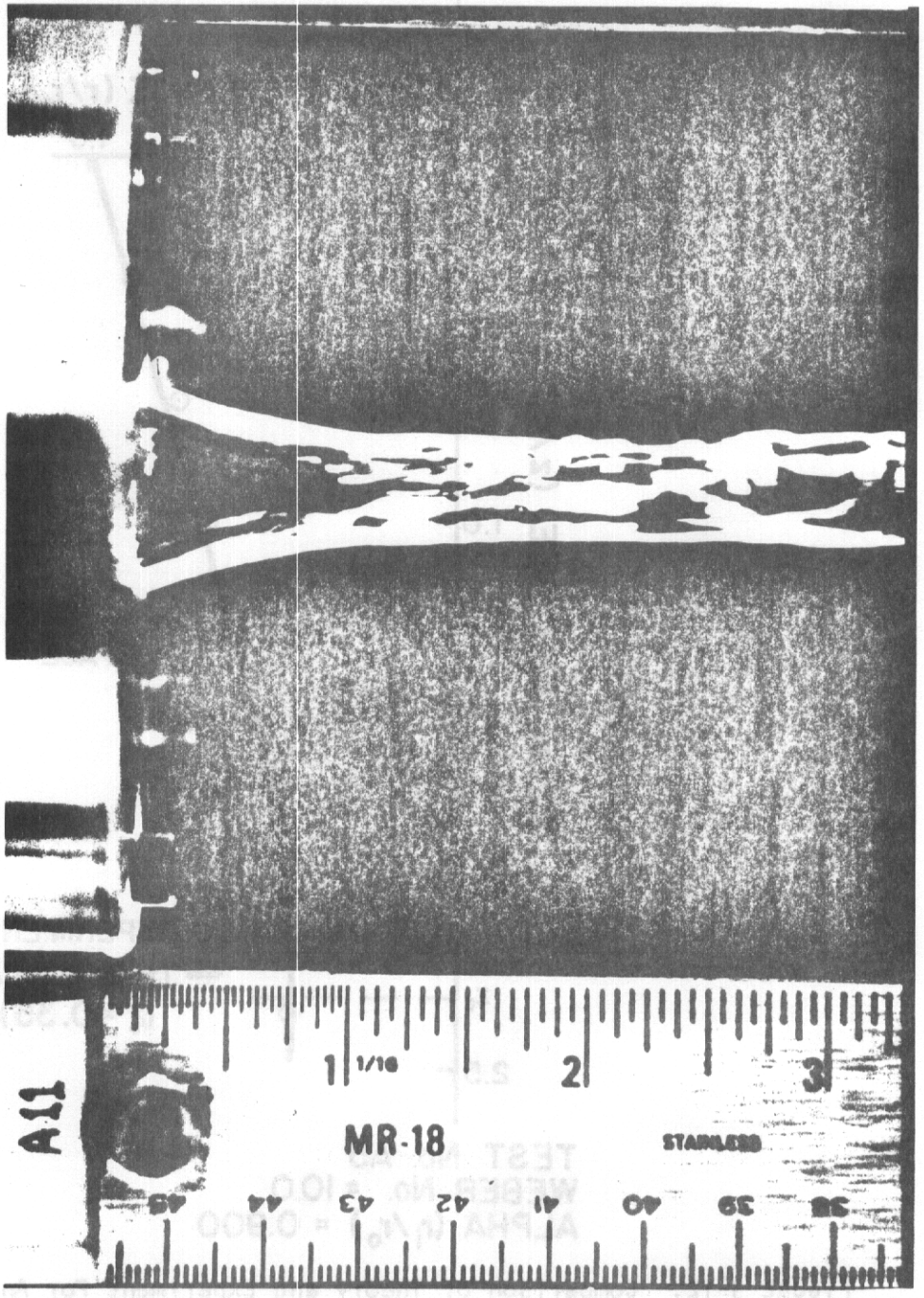

Figure 3-4. Annular Jet Without Air Injection: Nozzle A.

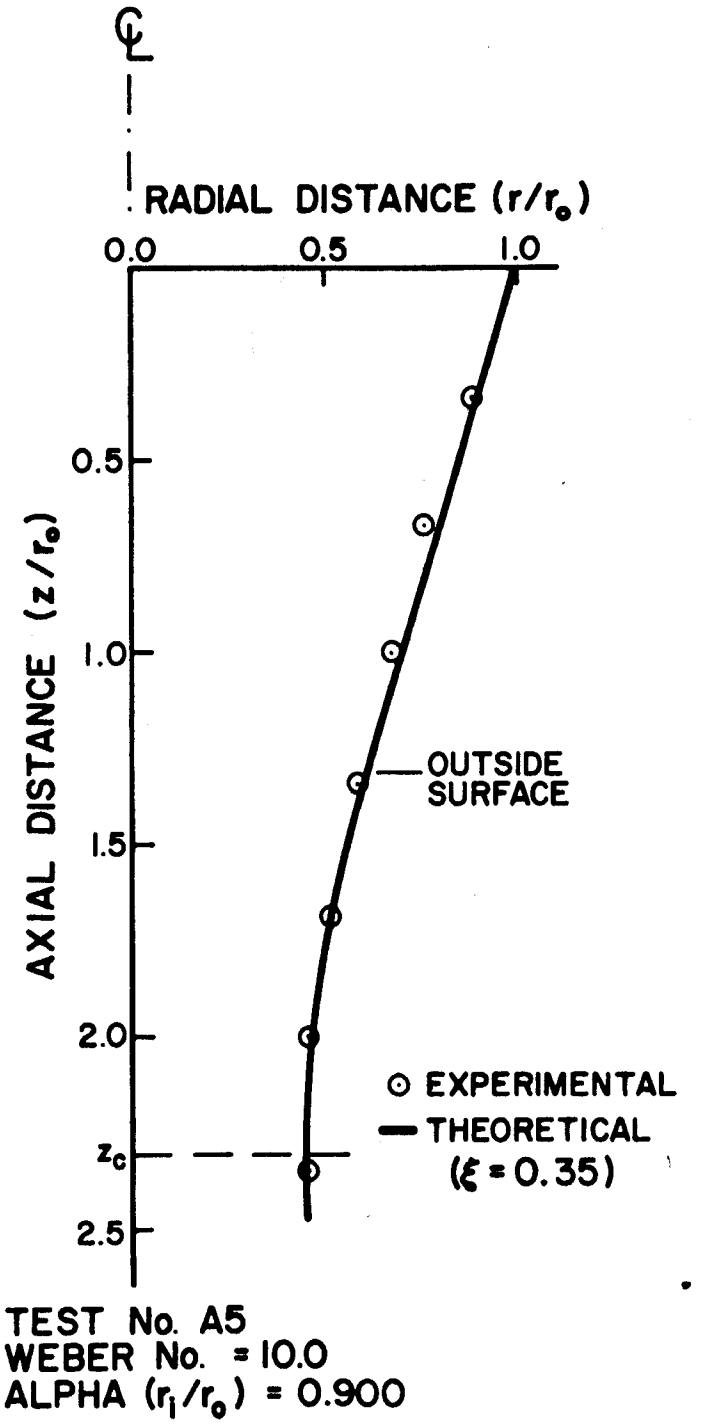

FIGURE 3-12. Comparison of Theory and Experiment For Annular Jets With No Air Injection: Nozzle A.

Figure 3-13 shows a photograph of an annular jet produced by nozzle B. Table 3-IV lists the experimental conditions for this test case. This annular jet has a thickness of 0.100 inches, and the curvature of the surface is not as pronounced as that of thinner jets. Figure 3-14 compares the experimental data points with the theoretical curve of the outside surface. Again we get excellent agreement.

TABLE 3-IV. Experimental Conditions for Nozzle B

Nozzle Characteristics

Outside Diameter = 1.000

Inside Diameter = 0.800

Aspect Ratio = 0.800

Flow Characteristics

Water Flow Rate = 619.5 gm/s

Air Flow Rate = vented to atmosphere

Water Velocity = 339.9 cm/s

Air Velocity = approximately zero

Water Temperature = 13.0^{o}C

Weber Number = 12.5

Figure 3-15 shows a photograph of an annular jet produced by nozzle C. Table 3-V lists the experimental conditions for this test case. Nozzle C produced an annular jet with a thickness of 0.150 inches, and the outside surface of the jet has considerably less curvature than the previous two cases. Figure 3-16 compares the

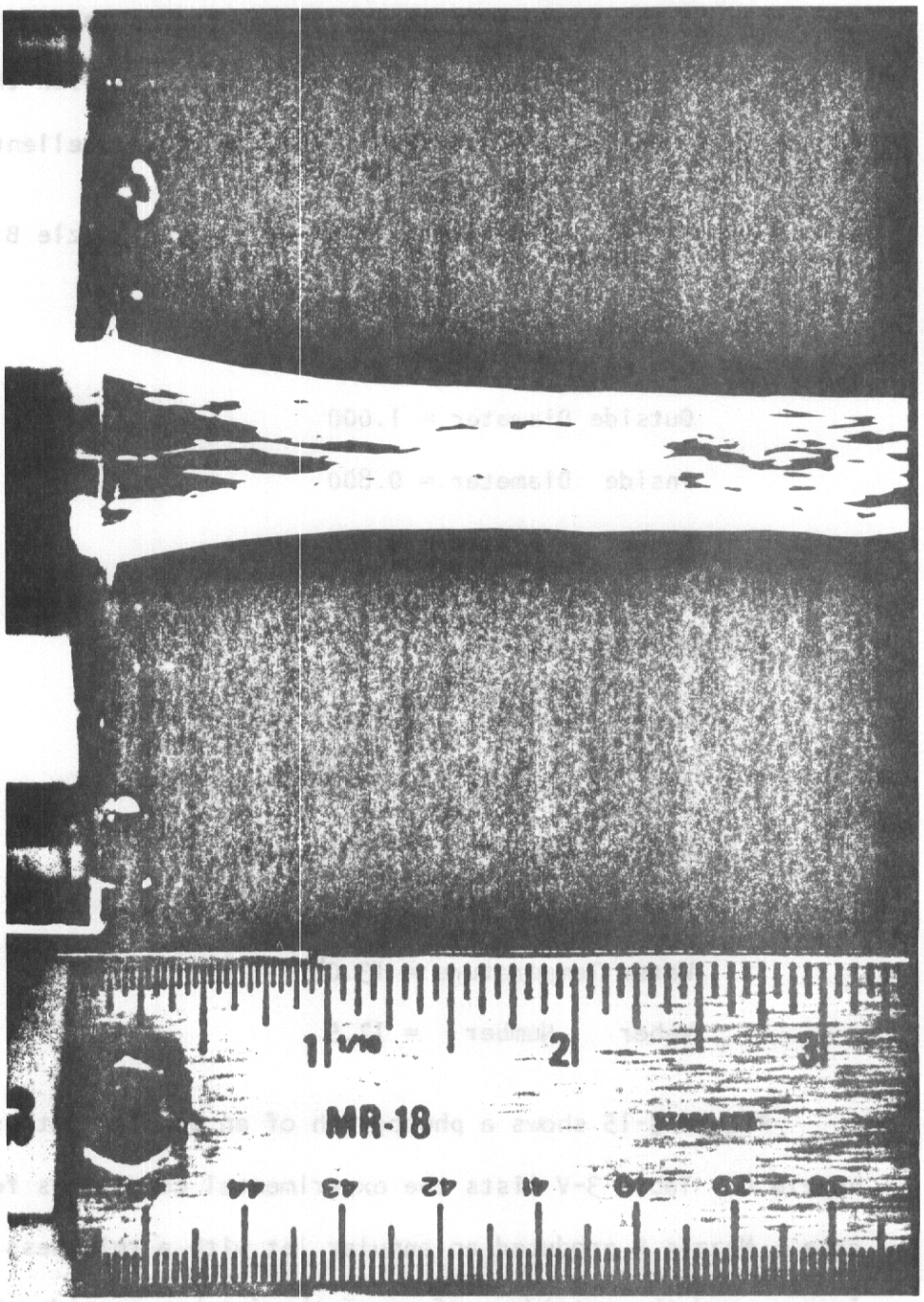

Figure 3-13. Annular Jet Without Air Injection: Nozzle B.

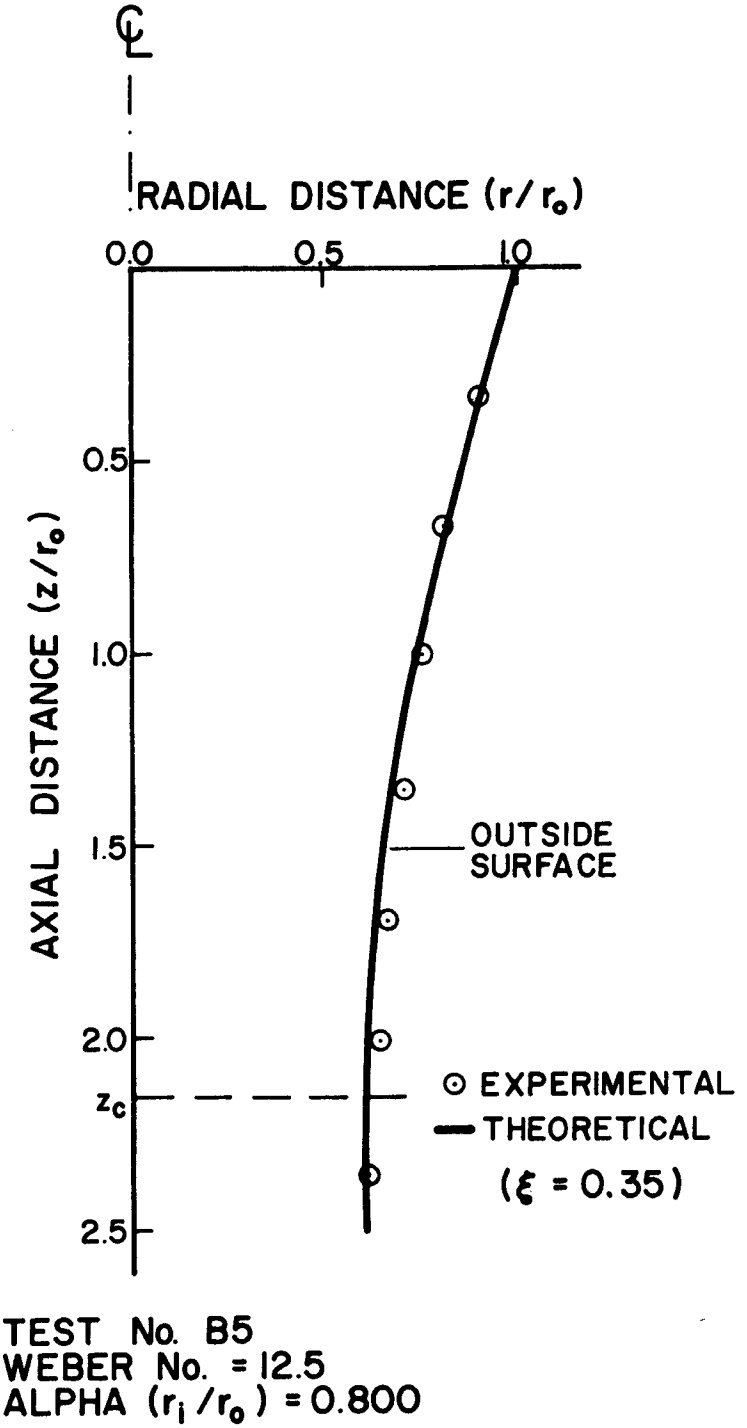

FIGURE 3-14. Comparison of Theory and Experiment For Annular Jets With No Air Injection: Nozzle B.

experimental data points with the theoretical curve. Once again the agreement is excellent.

TABLE 3-V. Experimental Conditions For Nozzle C

Nozzle Characteristics

Outside Diameter = 1.000

Inside Diameter = 0.700

Aspect Ratio = 0.700

Flow Characteristics

Water Flow Rate = 442.5 gm/s

Air Flow Rate = vented to atmosphere

Water Velocity = 171.4 cm/s

Air Velocity = approximately zero

Water Temperature = 13.0^{o}C

Weber Number = 7.7

One piece of information that is very difficult to obtain directly from the photographs is the distance the jet travels before it collapses into a solid circular jet. The inside surface of the jet is faintly visible in the photograph shown in Fig. 3-11, and becomes more obscure as the thickness of the jet increases as is evident by the photographs shown in Figures 3-13 and 3-15. However, the theoretical curves have been shown to be in excellent agreement with the experimental data points for the outside surface. Therefore, one expects the theoretical closure distances to be in agreement.

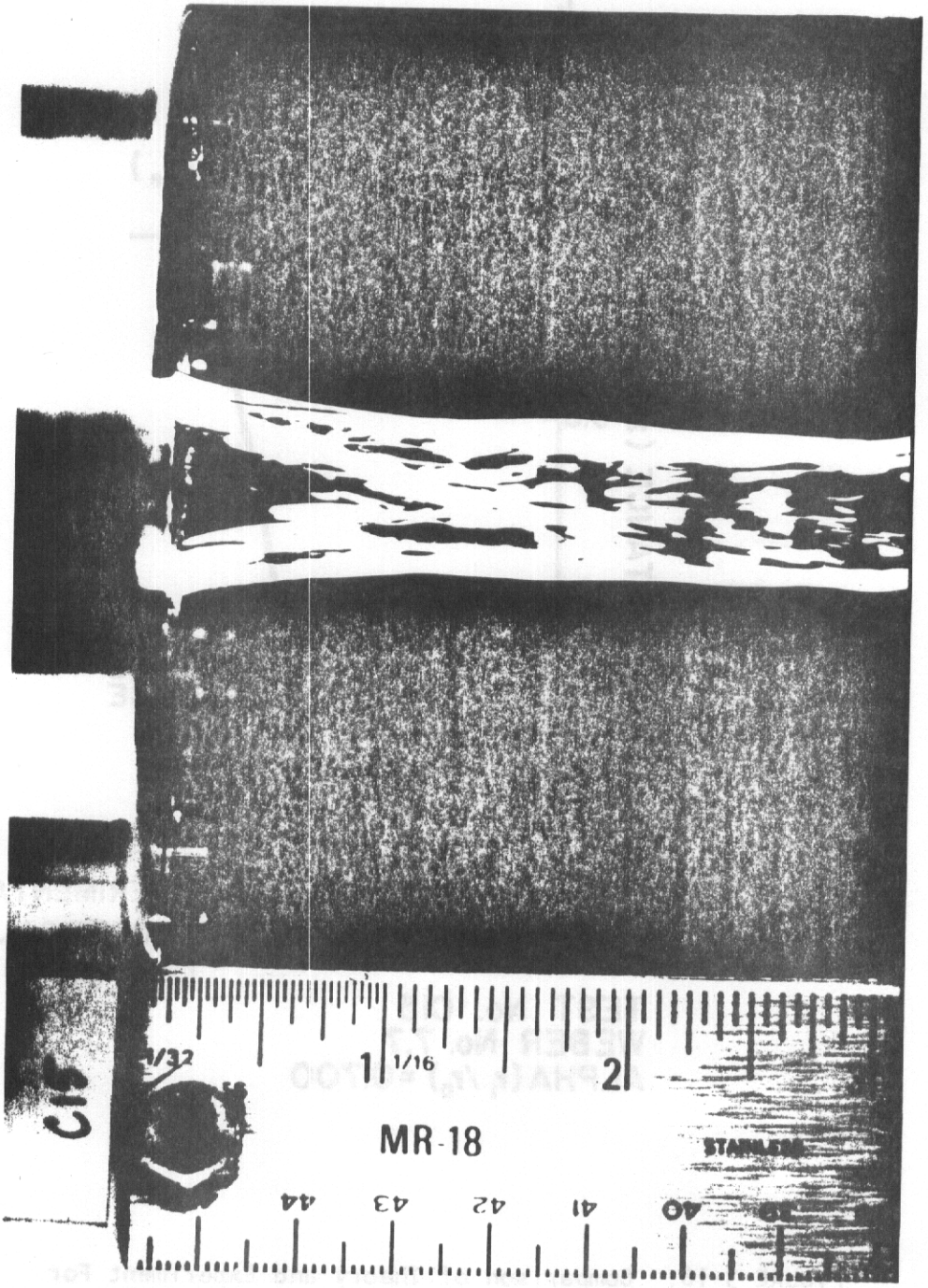

Figure 3-15. Annular Jet Without Air Injection: Nozzle C.

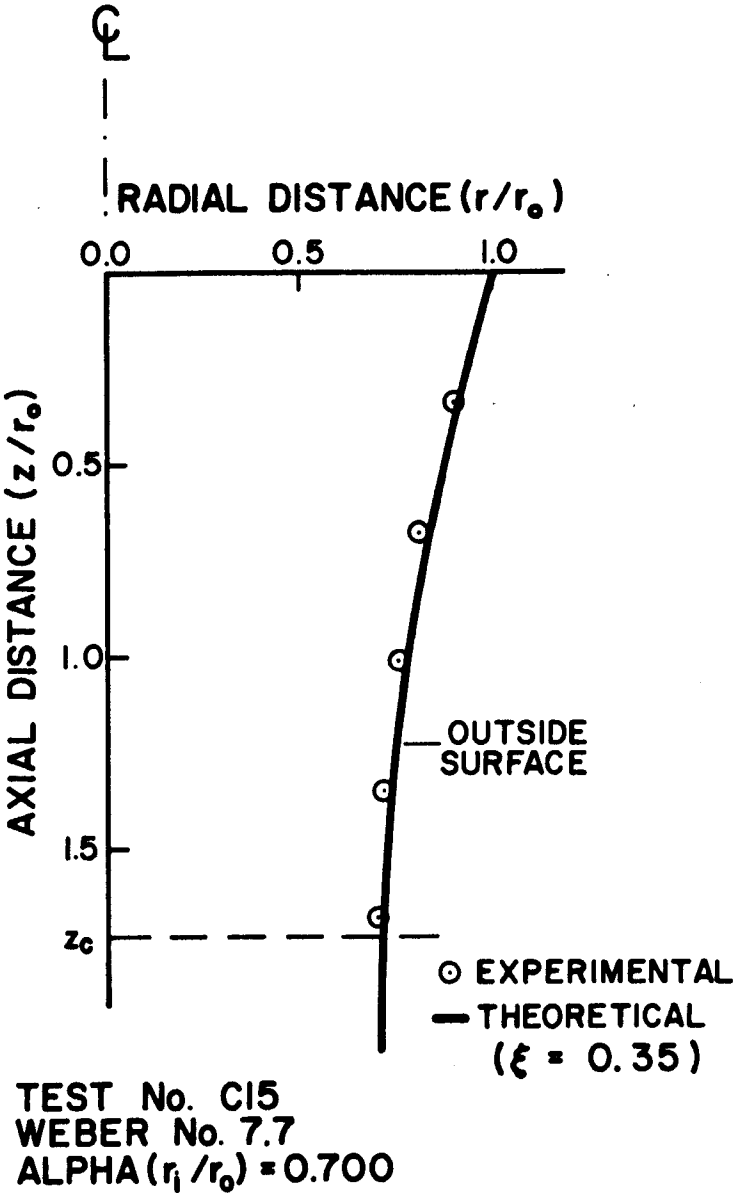

FIGURE 3-16. Comparison of Theory and Experiment For Annular Jets With No Air Injection: Nozzle C.

The theoretical closure distance can be obtained from Eqn. 4.33 by setting $\psi_1 = 0$, giving

$$\left(\frac{4}{Wb^2(1+\alpha)}\right) Z_c^2 + \xi Z_c - \alpha = 0 \tag{3.38}$$

where Z_c is the dimensionless closure distance,

$$Z_c = \frac{z}{r_0} \tag{3.39}$$

Therefore,

$$Z_c = \frac{Wb^2(1+\alpha)\xi}{8}\left[-1.0 + \sqrt{1.0 + \left(\frac{16\alpha}{Wb^2(1+\alpha)\xi^2}\right)}\right] \tag{3.40}$$

Figure 3-17 shows the theoretical closure distances predicted by Eqn. 3.40 as a function of both the Weber number and the aspect ratio. For Weber numbers greater than 50.0, the closure distances are determined almost entirely by the radial velocity component at the inlet section of the annular jet. For Weber numbers less than 50.0, the surface tension forces significantly affect the closure distance.

Figure 3-18 compares the theoretical closure distances with experimental results.

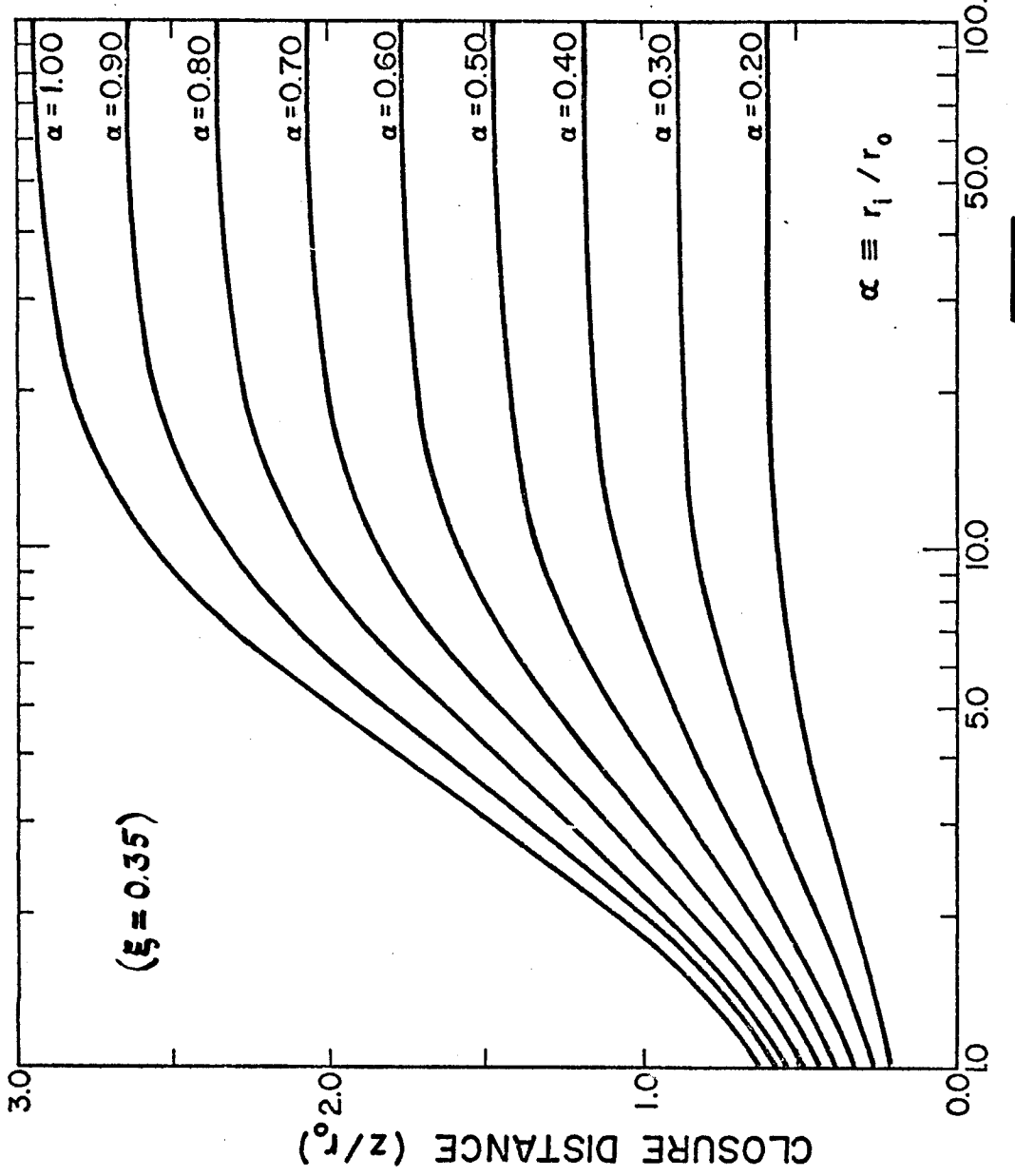

FIGURE 3-17. Theoretical Curves of Closure Distances For Annular Jets Produced by Sharp-Edged Orifice Nozzles.

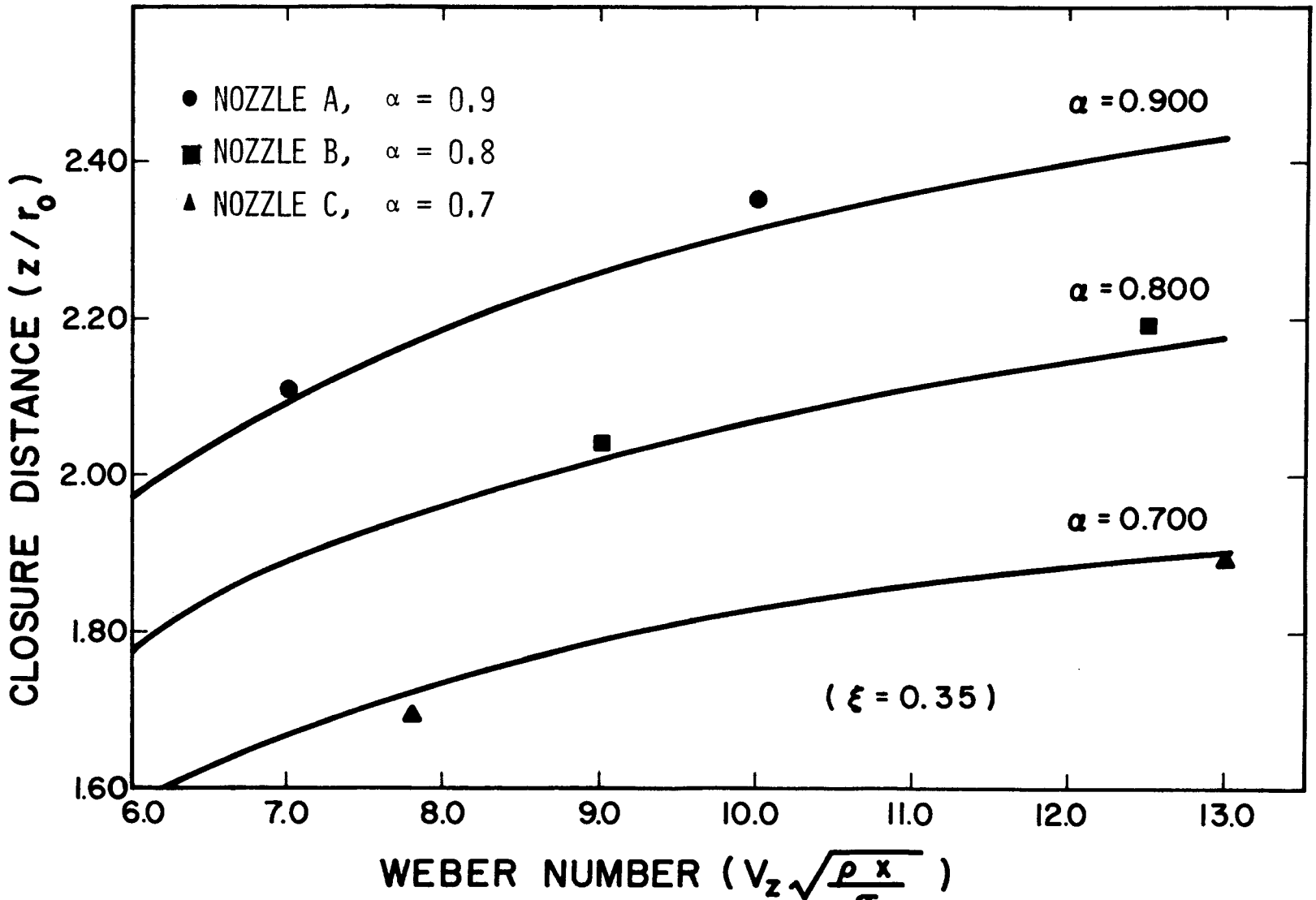

FIGURE 3-18. Comparison of Theoretical Closure Distances With Experimental Results.

CHAPTER 4

CONCLUSIONS AND RECOMMENDATIONS

4.1 Conclusions

Based on the theoretical and experimental results obtained in this investigation, the following conclusions can be drawn: An annular jet is unstable with respect to axisymmetric disturbances with wavelengths exceeding the circumference of the free surface. Since an annular jet has two free surfaces, the dispersion relations are maximized when the disturbances at each free surface have the same wavelength and are in phase. The maximum value of the amplification factor dominates the break-up of the jet, and this unstable mode causes the jet to break-up into spherical shells. The size and thickness of the spherical shells depends on the initial thickness of the annular jet, and the rate at which air is injected into the center of the annulus. This mode of jet break-up has been found experimentally (see Section 3.1).

The nozzle design, i.e. the initial velocity distribution in the jet, has a strong influence on the dynamics of annular jets. Annular jets produced by sharp-edged orifice nozzles have a nearly uniform velocity distribution across the jet, but possess a radial velocity component at the nozzle exit due to the fact that the streamlines are unable to bend abruptly around the orifice plates. On the other hand, annular jets produced by concentric cylinders sufficiently long to ensure a fully developed velocity profile across the jet are also expected to show contraction at the nozzle exit due to a

relaxation of the velocity profile. Only sharp-edged orifice nozzles have been tested in this investigation.

For annular jets produced by sharp-edged orifice nozzles, the jet collapses into a solid circular jet within 1 to 2 nozzle diameters when air is not injected into the center of the annulus. The closure distance depends on the radial velocity component of the jet at the nozzle exit, the jet Weber number, and the jet aspect ratio. Theoretical models used to predict the profile of the outside surface, and the jet closure distance agree very well with the experimental data.

4.2 Suggestions For Future Work

One of the first projects planned for the future is the testing of a concentric cylinder type nozzle. The nozzle will consist of two concentric cylinders which are long enough to ensure a fully developed velocity profile in the annular jet at the nozzle exit. Provisions will be made to inject air into the center of the annulus, and tests similar to those conducted with sharp-edged orifice nozzles will be performed.

Another interesting experiment will involve the study of the fluid behavior as it flows around objects of different shape placed in the annular jet to simulate a beam port such as that shown in Fig. 1-1. Does the annular jet reform after it passes over the rod? How much fluid is splattered by this disrupting influence? Can the effects be minimized by changing the design of the beam ports? These are a few of the questions that will be answered by this series of

experiments.

Also, methods to enhance the stability of liquid metal annular jets and prevent them from collapsing will be investigated.

NOMENCLATURE

English Symbols

i	=	imaginary number, ($i^2 = -1$)
I_m	=	modified Bessel function of the first kind of order m.
K_m	=	modified Bessel function of the second kind of order m.
k_1	=	axial wave number for the inside surface of the annular jet.
k_2	=	axial wave number for the outside surface of the annular jet.
m_1	=	azimuthal wave number for the inside surface of the annular jet.
m_2	=	azimuthal wave number for the outside surface of the annular jet.
p	=	perturbation pressure inside the annular jet.
p_1	=	perturbation pressure at the inside surface of the annular jet.
p_2	=	perturbation pressure at the outside surface of the annular jet.
P_o	=	static pressure inside the annular jet.
P_{o1}	=	static pressure due to surface tension of the fluid at the inside surface of the annular jet.
P_{o2}	=	static pressure due to the surface tension of the fluid at the outside surface of the annular jet.
r	=	radial distance in cylindrical coordinates.
r_1	=	radial distance to inside surface of the annular jet.
r_2	=	radial distance to the outside surface of the annular jet.
r_i	=	radius of the inside surface of the annular jet at the nozzle exit.

r_o = radius of the outside surface of the annular jet at the nozzle exit.

Re = Reynolds number.

R_1, R_2 = principal radii of curvature at a point on the free surface.

t = time.

u_r = radial component of the perturbation velocity.

$u_{\omega 1}$ = radial component of the perturbation velocity at the free surface ω_1.

$u_{\omega 2}$ = radial component of the perturbation velocity at the free surface ω_2.

v_z = axial velocity component of the annular jet.

Wb = Weber number, defined by Eqn. 3-30.

x_1 = unstable modes at the inside surface of the annular jet, $(x_1 = k_1 r_1)$.

x_2 = unstable modes at the outside surface of the annular jet, $(x_2 = k_2 r_2)$.

X = thickness of the annular jet, $(X = r_o - r_i)$.

z = axial distance in cylindrical coordinates.

z_c = closure distance of annular jet defined by Eqn. 3.39.

Greek Symbols

α = aspect ratio, $(\alpha = r_i/r_o)$.

δ = infinitesmal variation.

ε = initial value of the perturbation amplitude.

ε_1 = perturbation amplitude at the inside surface of the annular jet.

ε_2 = perturbation amplitude at the outside surface of the annular jet.

ζ = dimensionless axial distance, ($\zeta = z/r_o$)

η_1 = perturbation pressure problem at the inside surface of the annular jet, (see Eqn. 3.6).

η_2 = perturbation pressure problem at the outside surface of the annular jet (see Eqn. 3.6).

θ = angular displacement in cylindrical coordinates.

ν_1 = amplification factor for the inside surface of the annular jet, defined by Eqn. 3.17.

ν_2 = amplification factor for the outside surface of the annular jet, defined by Eqn. 3.18.

ξ = streamline slope of the inside surface of the annular jet at the nozzle exit, defined by Eqn. 3.22.

π = total perturbation pressure quantity defined by Eqn. 3.4.

ρ = fluid density.

σ = fluid surface tension.

ϕ = phase angle between disturbances at the two free surfaces of the annular jet.

ψ_1 = dimensionless radial distance to the inside surface of the annular jet, defined by Eqn. 3.34.

ψ_2 = dimensionless radial distance to the outside surface of the annular jet as defined by Eqn. 3.37.

Ψ = velocity potential for inviscid, irrotational, two-dimensional flow.

ω_1 = equation of the perturbed free surface on the inside of the annular jet, defined by Eqn. 3.1.

ω_2 = equation of the perturbed free surface on the outside of the annular jet, defined by Eqn. 3.2.

Ω_1 = perturbation pressure term for the inside free surface of the annular jet containing only the radial dependence, defined by Eqn. 3.11 a.

Ω_2 = perturbation pressure term for the outside free surface of the annular jet containing only the radial dependence, defined by Eqn. 3.11 b.

BIBLIOGRAPHY

1. Maniscalco, J.A. and Meier, W.R., "Liquid Lithium Waterfall Inertial Confinement Fusion Reactor Concept," Transactions of the American Nuclear Society, 26, New York, (June 1977).

2. Powell, J., Lazareth, O. and Fillo, J., "A Liquid-Wall Boiler and Moderator (BAM) for Heavy Ion-Pellet Fusion Reactors," Transactions of the American Nuclear Society, 26, New York, (June 1977).

3. Abdel-Khalik, S.I., Conn, R.W., and Moses, G.A., "Engineering Problems of Laser-Driven Fusion Reactors," presented in part at the 70th annual meeting of the American Institute of Chemical Engineers, New York, (Nov. 1977); accepted for publication in Nuclear Technology (1978).

4. Savart, "Mémoire sur la Constitution des Veines Liquides Lancées par des Orifices Circulaires en mince paroi," Ann. d. Chim. t. LIII. (1833) 337.

5. Plateau, "Statique Expérmentale et Theorique des Liquides soumis aux seules Forces Moleculaires, Paris, (1873), as cited by Lord Rayleigh in reference 6.

6. Rayleigh, Lord, "On the Instability of a Cylinder of Viscous Liquid under Capillary Force," Philosophical Magazine, XXXIV, pp. 145-154,(1892).

7. Rayleigh, Lord, "On the Instability of Cylindrical Fluid Surfaces," Philosophical Magazine, XXXIV, pp. 177-188 (1892).

8. Rayleigh, Lord, "On the Instability of Jets," Proceedings of the London Mathematical Society, 10, 4-13, (1879).

9. Rayleigh, Lord, "On the Capillary Phenomena of Jets," Proceedings of the Royal Society, 24, 71-97, (1879).

10. Goedde, E.F. and Yuen, M.C., "Experiments on Liquid Jet Instability," Journal of Fluid Mechanics, 40, part 3, 495-511 (1970).

11. Donnelly, R.J. and Glaberson, W., "Experiments on the Capillary Instability of a Liquid Jet," Proceeding of the Royal Society of London, A 290, 547-556, (1966).

12. Crane, L., Birch, S., and McCormack, P.D., "The Effect of Mechanical Vibration on the Break-up of a Cylindrical Water Jet in Air," British Journal of Applied Physics, 16, 743-750, (1964).

13. Crane, L., Birch, S. and McCormack, P.D., "An Experimental and Theoretical Analysis of Cylindrical Liquid Jets Subjected to Vibration," British Journal of Applied Physics, 16, 395-408, (1965).

14. Merrington, A.C. and Richardson, E.G., "The Break-Up of Liquid Jets," The Proceedings of the Physical Society, 59, part 1, 1-12 (1947).

15. Tyler, E. and Watkin, F., "Experiments with Capillary Jets," Philosophical Magazine, 14, No. 94, 849-881, (1932).

16. Tyler, E., "Instability of Liquid Jets," Philosophical Magazine, 16, No. 105, 505-519, (1933).

17. Smith, S.W.J., and Moss, H., Proceedings of the Royal Society, A, 93, 373, (1917).

18. Chandrasekhar, S., Hydrodynamic and Hydromagnetic Stability, Oxford Clarendon Press, (1961).

19. Wang, D.P., "Finite Amplitude Effect on the Stability of a Jet of Circular Cross-Section," Journal of Fluid Mechanics, 34, 299-313, (1968).

20. Yuen, M.C., "Non-Linear Capillary Instability of a Liquid Jet," Journal of Fluid Mechanics, 33, 151-163, (1968).

21. Lafrance, P., "Non-Linear Break-Up of a Laminar Liquid Jet," Physics of Fluids, Vol. 18, 428-432, (1974).

22. Tassoul, J.L., and Aubin, G., "Finite Amplitude Disturbances in Self-Gravitating Media," Journal of Mathematical Analysis and Applications, 45, 116-126, (1976).

23. Nayfeh, A.H., Physics of Fluids, 13, 841 (1970).

24. Phinney, R.E., "The Break-up of a Turbulent Liquid Jet in a Gaseous Atmosphere," Journal of Fluid Mechanics, Vol. 60, part 4, 689-701, (1973).

25. Chen, T.F. and Davis, J.R., "Disintegration of a Turbulent Water Jet," Proceedings A.S.C.E., HY 1, p. 175 (1964).

26. Fenn, R.W. and Middleman, S., "Newtonian Jet Stability: the role of Air Resistance," A. I. CH.E. J., 15, 379, (1969).

27. Grant, R.P. and Middleman, S., "Newtonian Jet Stability," A.I. Ch.E. J., 12, 669, (1966).

28. Miesse, C.C., "Correlation of Experimental Data on the Disintegration of Liquid Jets," Industrial and Engineering Chemistry, Vol. 47, No. 9, 1690-1701, (1955).

29. Lafrance, P., "The Breakup Length of Turbulent Liquid Jets," J.F.E. ASME, 414-415, (June 1977).

30. Hoyt, J.W. and Taylor, J.J., "Waves on Water Jets," J. Fluid Mech., Vol. 83, part 1, 119-127, (1977).

31. Middleman, S. and Gavis, J., "Expansion and Contractions of Capillary Jets of Newtonian Liquids," The Physics of Fluids, Vol. 4, No. 3, 355-359, (March 1961).

32. Bird, R. Byron, "The Change in Cross-Sectional Area of Jets as Analyzed by Macroscopic Balances," Rheology Research Center, The University of Wisconsin, RRC 23, (Feb. 1974).